Cramér–Rao Bounds for Estimating Range, Velocity, and Direction with an Active Array

Aleksandar Dogandžić, *Student Member, IEEE*, and Arye Nehorai, *Fellow, IEEE*

***Abstract*—We derive Cramér–Rao bound (CRB) expressions for the range (time delay), velocity (Doppler shift), and direction of a point target using an active radar or sonar array. First, general CRB expressions are derived for a narrowband signal and array model and a space-time separable noise model that allows both spatial and temporal correlation. We discuss the relationship between the CRB and ambiguity function for this model. Then, we specialize our CRB results to the case of temporally white noise and the practically important signal shape of a linear frequency modulated (chirp) pulse sequence. We compute the CRB for a three-dimensional (3-D) array with isotropic sensors in spatially white noise and show that it is a function of the array geometry only through the "moments of inertia" of the array. The volume of the confidence region for the target's location is proposed as a measure of accuracy. For this measure, we show that the highest (and lowest) target location accuracy is achieved if the target lies along one of the principal axes of inertia of the array. Finally, we compare the location accuracies of several array geometries.**

***Index Terms*—Cramér–Rao bound, radar array processing, sonar array processing.**

NOTATION

CPI	Coherent processing interval.
CRB	Cramér–Rao bound.
DOA	Direction of arrival.
SNR, SNR_1	Signal-to-noise ratio and SNR for a single pulse.
$\boldsymbol{a}(\boldsymbol{\theta})$	Array response vector.
c	Speed of propagation.
d_{MAX}	Maximum distance between array elements.
f_{B}	Bandwidth of the chirp signal.
m	Number of antennas in the array.
n, t, Δt	Sample index, continuous time, and sampling interval ($t = n\Delta t$).
n_τ, τ	Time delay in sampled and continuous time.
P	Number of pulses.
Q_{xx}, Q_{xy}, Q_{xz}, Q_{yy}, Q_{yz}	Spatial sensor distribution parameters, defining the "moment of inertia" tensor.
T_0	Duration of a single pulse.
T_{R}	Pulse repetition interval.
T_{CPI}	Duration of the coherent processing interval.
$h(t)$	Heaviside step function.
V_ζ	Volume of confidence ellipsoid for the target's location.
x	Complex amplitude of the received signal.
$\mathcal{A}([\boldsymbol{\theta}^T, \boldsymbol{v}^T]^T, [\boldsymbol{\theta}_0^T, \boldsymbol{v}_0^T]^T)$	DOA-range-velocity ambiguity function.
$\lambda, \Omega_{\text{c}}$	Carrier wavelength and angular carrier frequency in continuous time.
$\boldsymbol{\theta}$	Vector of DOA parameters.
$\boldsymbol{v}, \boldsymbol{\eta}$	Vectors containing time delay and Doppler shift in sampled and continuous time; $\boldsymbol{v} = [\omega_{\text{D}}, n_\tau]^T$, $\boldsymbol{\eta} = [\Omega_{\text{D}}, \tau]^T$.
$\boldsymbol{\zeta}, \boldsymbol{\alpha}$	Vector of target location parameters in Cartesian and spherical coordinates.
ϕ, ψ	Target's azimuth and elevation.
$n_\Sigma, \mathcal{N}_\Sigma$	Power spectral density of the noise (scalar and matrix).
ω_{D}, Ω_{D}	Doppler shift in sampled and continuous time.
ρ, v_{r}	Target's range and radial component of velocity.
Σ	Spatial noise covariance.
C	Temporal noise covariance.

Manuscript received March 6, 2000; revised February 12, 2001. This work was supported by the Air Force Office of Scientific Research under Grants F49620-99-1-0067 and F49620-00-1-0083, the National Science Foundation under Grant MIP-9615590, and the Office of Naval Research under Grant N00014-98-1-0542. The associate editor coordinating the review of this paper and approving it for publication was Prof. Jian Li.

The authors are with the Department of Electrical Engineering and Computer Science, University of Illinois at Chicago, Chicago, IL, 60607 USA (e-mail: nehorai@eecs.uic.edu).

Publisher Item Identifier S 1053-587X(01)03880-6.

I. INTRODUCTION

In active radar and sonar, a known waveform is transmitted, and the signal reflected from the target of interest is used to estimate its parameters. Typically, the received signal is modeled as a scaled, delayed, and Doppler-shifted version of the transmitted signal; see, e.g., [1]. Estimation of the time delay and Doppler shift provides information about the range and radial velocity of the target. For a single antenna, Cramér–Rao bound (CRB) expressions for the range (i.e., time delay) and velocity (i.e., Doppler shift) have been extensively studied in the radar literature [1, ch. 10.2], [2], [3]. However, recent advances in radar signal processing are associated with the use of antenna arrays [4]–[7].

Compared with a single sensor, a sensor array guarantees more accurate range and velocity estimation. Furthermore, it allows estimation of the target's direction. Thus, it is of interest to

compute CRB expressions for active sensor arrays. Some work in this direction has already been done in [7] and [8], where CRB expressions for the direction and Doppler shift were derived for a radar array model in which conversion to baseband and matched filtering (i.e., pulse compression) had been performed at each antenna.

In this paper (see also [9]), we consider a narrowband signal and array model prior to matched filtering, i.e., only after the conversion to baseband. In [10], we presented maximum likelihood (ML) methods for this model and for unknown spatially correlated and temporally white noise. Unlike [7] and [8], our signal model allows estimation of the time delay.[1] Due to the narrowband array assumption, the received signal is "space-time separable," as defined in [11]. We assume a space-time separable noise model as well (following [11]), which is relatively general and allows both spatial and temporal noise correlation. Under these signal and noise models, we compute the CRB expressions for the time delay, direction, and Doppler shift. Owing to the more general signal and noise structure, our CRB results for direction parameters and Doppler shift generalize those in [7]. Furthermore, our CRB expressions for the time delay and Doppler shift extend the classical radar CRB results in [1, ch. 10.2] and [3] and to a sensor array.

Signal and noise models are explained in detail in Section II. In Section III, CRB expressions for these models are presented. We show that the CRB for the direction parameters is independent of whether or not the time delay and Doppler shift are known, and vice versa; see Section III-A. This independence is a consequence of the space-time separable structure of the adopted signal and noise models. We discuss the relationship between the ambiguity function and CRB in Section III-B. Then, we examine in more detail the case of temporally white noise (see Section III-C) and a linear frequency modulated (chirp) pulse sequence (see Section III-C2. In Section IV, we compute and analyze the CRB for the target's location in spatially white noise when the array consists of identical isotropic sensors. Using the volume of the confidence region for the target's location as an accuracy measure and assuming both spatially and temporally white noise, we show that the highest accuracy is achieved for targets lying along one of the principal axes of inertia of the array; an analogous result holds for the lowest accuracy. Finally, we compare the location accuracies of several three-dimensional (3-D) array geometries.

II. Signal and Noise Models

We present the signal and noise models used in this paper as well as the underlying assumptions needed for their validity.

Suppose an m-element antenna array receives a scaled, time-delayed, and Doppler-shifted echo of a known complex bandpass signal $s(t)\exp(j\Omega_c t)$, where Ω_c is the angular carrier frequency. Knowing the time delay τ and Doppler shift Ω_D (and assuming a target with constant radial velocity), the target's range and radial component of velocity are determined by $\rho = c\tau/2$ and $v_r = \Omega_D c/(2\Omega_c)$, where c is the wave propagation speed; see e.g., [1, ch. 9.1]. We define a sample $s[n]$ of a continuous-time signal $s(t)$ as $s[n] = s(n\Delta t)$, where Δt is the sampling interval, and $t = n\Delta t$. We define the time delay and Doppler shift in the sampled signal domain as $n_\tau = \tau/\Delta t$ and $\omega_D = \Omega_D \cdot \Delta t$, respectively.

After converting to baseband and sampling, the signal received by the array at time $n\Delta t$ becomes

$$\boldsymbol{y}[n] = \boldsymbol{a}(\boldsymbol{\theta}) \cdot x \cdot \exp(j\omega_D n) s[n - n_\tau] + \boldsymbol{e}[n] \qquad (2.1)$$

for $n = 1, \cdots, N$, where

- x complex amplitude of the signal;
- $\boldsymbol{a}(\boldsymbol{\theta})$ $m \times 1$ vector of the array response to a plane wave reflected from the target;
- $\boldsymbol{e}[n]$ additive noise.

Here, $\boldsymbol{\theta}$ is the vector of the direction-of-arrival (DOA) parameters (and may contain additional parameters, such as polarization coefficients; see [12]). We assume that the snapshots taken at $n = 1, \cdots, N$ cover the whole of a coherent processing interval (CPI). Therefore, the time duration of the CPI is $T_{CPI} = N\Delta t$. We model the complex amplitude x as an unknown deterministic constant during the CPI; see also [7] and [8]. (In reality, $|x|$ is inversely proportional to the square of range ρ, but we ignore this dependence throughout; see also Section IV-A). Moreover, the target's direction, range, and radial component of velocity are also modeled as unknown deterministic constants within the CPI.

Note that although n is chosen to be an integer due to sampling, n_τ and $n - n_\tau$ are not necessarily integers. Therefore, $s[n - n_\tau]$ is a function of a real argument $n - n_\tau$, evaluated for integer values of n.

For the model in (2.1) to be valid, several assumptions need to be satisfied. To model the Doppler effect by a frequency shift, the radial component of the target's velocity needs to be much smaller than the propagation speed (i.e., $v/c \ll 1$), and the time-bandwidth product of the complex envelope $s(t)$ should be much smaller than $c/(2v)$; see also [1, ch. 9, eqs. (19) and (23)]. We refer to the above assumptions as the *narrowband signal assumptions*. In addition, it is assumed that the propagation time of the signal across the array is much smaller than the reciprocal of the signal bandwidth, which is the standard narrowband assumption in array processing (or *narrowband array assumption*). It is important to observe that the narrowband array assumption implies that the range estimation accuracy cannot be better than the array size along the direction to the target. In other words, the CRB for the time-delay estimation is valid only if it is larger than the (square of the) propagation time of the signal across the array.

Equation (2.1) generalizes the radar target model in [1, ch. 9 and 10] to account for multiple sensors, thus enabling DOA estimation. However, we assume that the complex amplitude x is deterministic (as in [7] and [8]), whereas in [1, ch. 9 and 10], x was modeled as a zero-mean Gaussian random variable. Since we consider the measurements collected in one CPI only, we do not need to make any assumption concerning the distribution of x from one CPI to another.

[1]Note that the model "after matched filtering" in [7] and [8] is based on assumptions that the time delay is known, noise is temporally white within a pulse, and the waveform ambiguity function is insensitive to the Doppler shift; see [8, pp. 14 and 15]. Here, we do not need these assumptions.

Define the vector of unknown target parameters $\boldsymbol{\gamma} = [\mathrm{Re}\{x\}, \mathrm{Imag}\{x\}, \boldsymbol{\theta}^T, \boldsymbol{\upsilon}^T]^T$, where $\boldsymbol{\upsilon} = [\omega_{\mathrm{D}}, n_\tau]^T$. Define also the noise-free signal vector at the nth sample as $\boldsymbol{\mu}[n, \boldsymbol{\gamma}] = \boldsymbol{a}(\boldsymbol{\theta}) \cdot x \cdot \exp(j\omega_{\mathrm{D}} n) s[n - n_\tau]$. Stacking all N samples into a single vector, (2.1) can be rewritten as

$$\boldsymbol{y} = \boldsymbol{\mu}(\boldsymbol{\gamma}) + \boldsymbol{e} = x \cdot \boldsymbol{\phi}(\boldsymbol{\upsilon}) \otimes \boldsymbol{a}(\boldsymbol{\theta}) + \boldsymbol{e} \tag{2.2}$$

where $\otimes$ denotes the Kronecker product, and

$$\boldsymbol{y} = [\boldsymbol{y}[1]^T, \boldsymbol{y}[2]^T \cdots \boldsymbol{y}[N]^T]^T \tag{2.3a}$$

$$\boldsymbol{\mu}(\boldsymbol{\gamma}) = [\boldsymbol{\mu}(1, \boldsymbol{\gamma})^T, \boldsymbol{\mu}(2, \boldsymbol{\gamma})^T \cdots \boldsymbol{\mu}(N, \boldsymbol{\gamma})^T]^T \tag{2.3b}$$

$$\boldsymbol{\phi}(\boldsymbol{\upsilon}) = [s[1 - n_\tau] \exp(j\omega_{\mathrm{D}} 1), s[2 - n_\tau] \exp(j\omega_{\mathrm{D}} 2) \cdots, s[N - n_\tau] \exp(j\omega_{\mathrm{D}} N)]^T \tag{2.3c}$$

$$\boldsymbol{e} = [\boldsymbol{e}[1]^T, \boldsymbol{e}[2]^T \cdots \boldsymbol{e}[N]^T]^T. \tag{2.3d}$$

The additive noise term $\boldsymbol{e}$ models interference due to clutter, receiver noise, and jamming. When dominated by clutter or jamming, the noise $\boldsymbol{e}$ is usually both temporally and spatially correlated. We assume that $\boldsymbol{e}$ is zero-mean Gaussian, spatially and temporally correlated with spatio-temporal covariance

$$\mathrm{E}[\boldsymbol{e}\boldsymbol{e}^*] = C \otimes \Sigma \tag{2.4}$$

where

C and Σ	noise temporal and spatial covariance matices;
$\mathrm{E}[\cdot]$	expectation;
"*"	conjugate transpose.

These matrices are assumed to be positive definite and independent of the target parameters $\boldsymbol{\gamma}$; thus, the signal and noise parameters are disjoint. This is a relatively general model for the noise covariance, which includes as special cases the jamming and receiver noise models developed in [6, ch. 2]. The above model can successfully model clutter if the scatterers move with a constant radial velocity; see [11, sec. VI] (in practical cases, this condition usually holds if scatterers are not moving, i.e., their radial velocity is zero; see also the discussion in [11, sec. VI]). Interestingly, it has also been recently proposed to model noise and interference in wireless communication systems [13].

Note that the signal and noise models in (2.2) and (2.4) satisfy the space-time separability conditions in [11, eqs. (10) and (11)]. The signal model is separable with respect to the "space" (DOA) parameters $\boldsymbol{\theta}$ and "time" parameters $\boldsymbol{\upsilon}$ since the received signal is modeled as the product of a function of $\boldsymbol{\theta}$ and a function of $\boldsymbol{\upsilon}$ (which is a consequence of the narrowband array assumption; see also [11, sec. IV]). Similarly, the noise model is separable since the noise covariance is the product of a "spatial" and a "temporal" covariance. In passive systems, space-time separability has been considered in [14, sec. IV]. A separable model offers significant computational savings since the estimation procedure can be decoupled [7], [11], [14]. In the following section, we present the CRB and the ambiguity function for these models and show that they are separable as well.

III. General CRB Results

We present the CRB results for signal and noise models in Section II. The CRB and ambiguity results derived in Section III-A and Section III-B are valid for a general class of separable signal and noise models, described by (2.2) and (2.4). In Section III-B, we establish the relationship between the ambiguity function and the CRB. Then, in Section III-C, we simplify the CRB to a special case of narrowband array and signal model in (2.1) and temporally white noise. Finally, in Section III-C2, we further specialize these results to the practically important signal shape of a rectangular chirp pulse sequence in continuous time.

A. CRB Expressions for Spatially and Temporally Correlated Noise

In Appendix A, we derive the CRB matrix expressions for $\boldsymbol{\theta}$ and $\boldsymbol{\upsilon}$ under the signal and noise models (2.2) and (2.4), respectively. The results are

$$\mathrm{CRB}_{\theta\theta} = \frac{1}{2|x|^2 \cdot \boldsymbol{\phi}(\boldsymbol{\upsilon})^* C^{-1} \boldsymbol{\phi}(\boldsymbol{\upsilon})} \cdot \left[\mathrm{Re} \left\{ \frac{\partial \boldsymbol{a}(\boldsymbol{\theta})^*}{\partial \boldsymbol{\theta}} \Sigma^{-1/2} \Pi_a^{\perp}(\boldsymbol{\theta}, \Sigma) \Sigma^{-1/2} \frac{\partial \boldsymbol{a}(\boldsymbol{\theta})}{\partial \boldsymbol{\theta}^T} \right\} \right]^{-1} \tag{3.1a}$$

$$\mathrm{CRB}_{\boldsymbol{\upsilon}\theta} = 0 \tag{3.1b}$$

$$\mathrm{CRB}_{\boldsymbol{\upsilon}\boldsymbol{\upsilon}} = \begin{bmatrix} \mathrm{CRB}_{\omega_{\mathrm{D}}\omega_{\mathrm{D}}} & \mathrm{CRB}_{n_\tau \omega_{\mathrm{D}}} \\ \mathrm{CRB}_{n_\tau \omega_{\mathrm{D}}} & \mathrm{CRB}_{n_\tau n_\tau} \end{bmatrix} = \frac{1}{2|x|^2 \cdot \boldsymbol{a}(\boldsymbol{\theta})^* \Sigma^{-1} \boldsymbol{a}(\boldsymbol{\theta})} \cdot \left[\mathrm{Re} \left\{ \frac{\partial \boldsymbol{\phi}(\boldsymbol{\upsilon})^*}{\partial \boldsymbol{\upsilon}} C^{-1/2} \Pi_{\boldsymbol{\phi}}^{\perp}(\boldsymbol{\upsilon}, C) C^{-1/2} \frac{\partial \boldsymbol{\phi}(\boldsymbol{\upsilon})}{\partial \boldsymbol{\upsilon}^T} \right\} \right]^{-1} \tag{3.1c}$$

where

$$\Pi_a^{\perp}(\boldsymbol{\theta}, \Sigma) = I_m - \frac{1}{\boldsymbol{a}(\boldsymbol{\theta})^* \Sigma^{-1} \boldsymbol{a}(\boldsymbol{\theta})} \cdot \Sigma^{-1/2} \boldsymbol{a}(\boldsymbol{\theta}) \boldsymbol{a}(\boldsymbol{\theta})^* \Sigma^{-1/2} \tag{3.2a}$$

$$\Pi_{\phi}^{\perp}(\boldsymbol{\upsilon}, C) = I_N - \frac{1}{\boldsymbol{\phi}(\boldsymbol{\upsilon})^* C^{-1} \boldsymbol{\phi}(\boldsymbol{\upsilon})} \cdot C^{-1/2} \boldsymbol{\phi}(\boldsymbol{\upsilon}) \boldsymbol{\phi}(\boldsymbol{\upsilon})^* C^{-1/2}. \tag{3.2b}$$

Here, I_N denotes the identity matrix of size N, $\Sigma^{1/2}$ denotes a Hermitian square root of a Hermitian matrix Σ, and $\Sigma^{-1/2} = (\Sigma^{1/2})^{-1}$; we will use this notation throughout the paper.

Observe that the CRB for $\boldsymbol{\theta}$ and $\boldsymbol{\upsilon}$ is block-diagonal [see (3.1b)] and therefore decoupled, i.e., $\mathrm{CRB}_{\boldsymbol{\upsilon}\boldsymbol{\upsilon}}$ remains the same whether or not $\boldsymbol{\theta}$ is known, and similarly, $\mathrm{CRB}_{\theta\theta}$ is the same whether or not $\boldsymbol{\upsilon}$ is known; see Appendix A. This result is somewhat unexpected since the Fisher information matrix (FIM) for the target parameters $\boldsymbol{\gamma}$ is not block diagonal; see (A.2) and (A.3) in Appendix A. The decoupling is a consequence of the assumed space-time separability of signal and noise models and the assumption of the complex amplitude x as an unknown deterministic constant. [For example, for known x, the CRB for $\boldsymbol{\theta}$ and $\boldsymbol{\upsilon}$ would not be block-diagonal, and $\mathrm{CRB}_{\boldsymbol{\upsilon}\boldsymbol{\upsilon}}$ and $\mathrm{CRB}_{\theta\theta}$ would not be decoupled.] In addition, since the signal and additive noise parameters are disjoint, the above CRB expressions hold regardless of whether the spatio-temporal noise covariance $C \otimes \Sigma$ is known or unknown.

If the temporal noise covariance C is known and the spatial noise covariance Σ is unknown, the above CRBs will be reached asymptotically in time (i.e., as $N \to \infty$) by the ML estimation procedure; see e.g., [15, sec. 7.5]. For unknown temporal covariance C, it is important to carefully choose its structure so that the number of parameters characterizing it will not depend on time (otherwise, if the number of parameters increases with N, estimation algorithms may not be able to attain the CRB as $N \to \infty$). Such a model for C may be obtained, for example, if the noise is stationary [i.e., the (n_1, n_2)th entry of C, denoted by C_{n_1,n_2}, depends only on $n_1 - n_2$] and the correlation between the snapshots decreases to zero for a sufficiently large time difference (i.e., $C_{n_1,n_2} = 0$ for $|n_1 - n_2|$ greater than a certain threshold).

Due to the symmetry in the signal representation [with respect to $\boldsymbol{\phi}(\boldsymbol{v})$ and $\boldsymbol{a}(\boldsymbol{\theta})$; see (2.2)] and noise parametrization [with respect to C and Σ; see (2.4)], there is a duality between (3.1a) and (3.1c). One expression can be obtained from the other by interchanging the spatial covariance matrix Σ, array response vector $\boldsymbol{a}(\boldsymbol{\theta})$, and its derivative $\partial \boldsymbol{a}(\boldsymbol{\theta})/\partial \boldsymbol{\theta}^T$ with the temporal covariance matrix C, temporal steering vector $\boldsymbol{\phi}(\boldsymbol{v})$, and its derivative $\partial \boldsymbol{\phi}(\boldsymbol{v})/\partial \boldsymbol{v}^T$, respectively.

1) CRB on the Target's Radial Velocity for a Moving Array: We consider the practically important case of a moving array and compute the CRB on the target's radial velocity. We show that this CRB depends on the CRB for direction parameters; thus, the decoupling result from previous section is invalid in this case.

Let us assume that the array moves with constant velocity. Then, the Doppler shift due to the radial component of the target's velocity (in the sampled-signal domain) is

$$\omega_{\mathrm{DT}} = 2\Omega_{\mathrm{c}} \Delta t/c \cdot v_{\mathrm{Tr}} = \omega_{\mathrm{D}} + \omega_{\mathrm{D}A} \cos[\varphi(\boldsymbol{\theta})] \tag{3.3}$$

where

ω_{D}	(relative) Doppler shift measured by the array;
$\omega_{\mathrm{D}A} \cos[\varphi(\boldsymbol{\theta})]$	Doppler shift due to the array movement and $\omega_{\mathrm{D}A} = 2\Omega_{\mathrm{c}} \Delta t/c \cdot v_A$;
v_{Tr}	radial component of target's velocity;
v_A	magnitude of the vector of array velocity;
$\varphi = \varphi(\boldsymbol{\theta})$	angle between the array velocity vector and the vector of direction to the target.

See Fig. 1. Note that ω_{DT} is a function of both $\boldsymbol{\theta}$ and ω_{D}, but we omit these dependencies for notational simplicity. In Appendix A1, we derive the CRB for ω_{DT} as

$$\begin{aligned} \mathrm{CRB}_{\omega_{\mathrm{DT}}\omega_{\mathrm{DT}}} &= \mathrm{CRB}_{\omega_{\mathrm{D}}\omega_{\mathrm{D}}} + \omega_{\mathrm{D}A}^2 \cdot \sin^2[\varphi(\boldsymbol{\theta})] \\ &\quad \cdot \frac{\partial \varphi(\boldsymbol{\theta})}{\partial \boldsymbol{\theta}^T} \mathrm{CRB}_{\theta\theta} \frac{\partial \varphi(\boldsymbol{\theta})}{\partial \boldsymbol{\theta}} \\ &= \mathrm{CRB}_{\omega_{\mathrm{D}}\omega_{\mathrm{D}}} + \omega_{\mathrm{D}A}^2 \cdot \sin^2[\varphi(\boldsymbol{\theta})] \cdot \mathrm{CRB}_{\varphi\varphi} \end{aligned} \tag{3.4}$$

where $\mathrm{CRB}_{\varphi\varphi}$ denotes the CRB for estimating φ, and$\mathrm{CRB}_{\omega_{\mathrm{D}}\omega_{\mathrm{D}}}$ is the CRB for estimating ω_{D}; see (3.1c). The second term in (3.4) can be neglected if the array velocity is small (then $\omega_{\mathrm{D}A}$ is small) or the angle $\varphi(\boldsymbol{\theta})$ between the array velocity and the target's direction is small. Then, $\mathrm{CRB}_{\omega_{\mathrm{D}}\omega_{\mathrm{D}}}$ is a good measure of the achievable accuracy for estimating the target's radial velocity. Note that $\mathrm{CRB}_{\omega_{\mathrm{D}}\omega_{\mathrm{D}}} \leq \mathrm{CRB}_{\omega_{\mathrm{DT}}\omega_{\mathrm{DT}}}$, i.e., $\mathrm{CRB}_{\omega_{\mathrm{D}}\omega_{\mathrm{D}}}$ can be viewed as a lower bound on $\mathrm{CRB}_{\omega_{\mathrm{DT}}\omega_{\mathrm{DT}}}$.

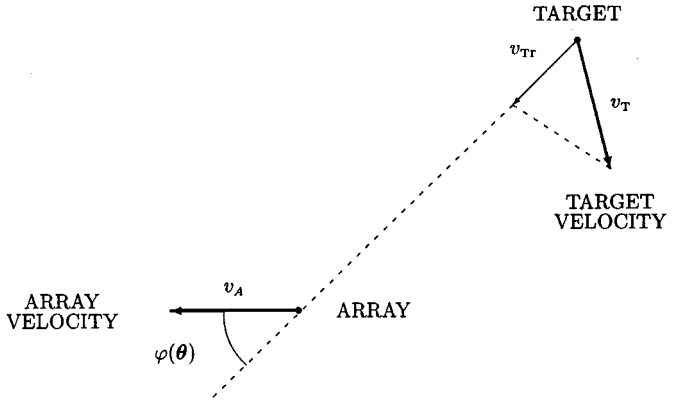

Fig. 1. Moving array.

B. CRB and Ambiguity Function

We now establish the relationship between the ambiguity function and the CRB. Unlike the CRB, which is a local measure of estimation accuracy, the ambiguity function is used to assess the global resolution and large error properties of the estimates [1], [16]. For the following discussion, it is useful to define the signal-to-noise ratio (SNR) as

$$\mathrm{SNR} = |x|^2 \cdot \boldsymbol{\phi}(\boldsymbol{v})^* C^{-1} \boldsymbol{\phi}(\boldsymbol{v}) \cdot \boldsymbol{a}(\boldsymbol{\theta})^* \Sigma^{-1} \boldsymbol{a}(\boldsymbol{\theta}). \tag{3.5}$$

Assume that we have two targets with parameters $\boldsymbol{\theta}$, $\boldsymbol{v}$, and $\boldsymbol{\theta}_0$, $\boldsymbol{v}_0$, respectively. The *DOA-range-velocity ambiguity function* can be easily derived using [16, def. 2]

$$\mathcal{A}([\boldsymbol{\theta}^T, \boldsymbol{v}^T]^T, [\boldsymbol{\theta}_0^T, \boldsymbol{v}_0^T]^T) = \mathcal{A}(\boldsymbol{v}, \boldsymbol{v}_0) \cdot \mathcal{A}(\boldsymbol{\theta}, \boldsymbol{\theta}_0) \tag{3.6}$$

where

$$\mathcal{A}(\boldsymbol{v}, \boldsymbol{v}_0) = \frac{|\boldsymbol{\phi}(\boldsymbol{v}_0)^* C^{-1} \boldsymbol{\phi}(\boldsymbol{v})|^2}{\boldsymbol{\phi}(\boldsymbol{v}_0)^* C^{-1} \boldsymbol{\phi}(\boldsymbol{v}_0) \cdot \boldsymbol{\phi}(\boldsymbol{v})^* C^{-1} \boldsymbol{\phi}(\boldsymbol{v})} \tag{3.7a}$$

$$\mathcal{A}(\boldsymbol{\theta}, \boldsymbol{\theta}_0) = \frac{|\boldsymbol{a}(\boldsymbol{\theta}_0)^* \Sigma^{-1} \boldsymbol{a}(\boldsymbol{\theta})|^2}{\boldsymbol{a}(\boldsymbol{\theta}_0)^* \Sigma^{-1} \boldsymbol{a}(\boldsymbol{\theta}_0) \cdot \boldsymbol{a}(\boldsymbol{\theta})^* \Sigma^{-1} \boldsymbol{a}(\boldsymbol{\theta})} \tag{3.7b}$$

see Appendix B. An analogous expression for the ambiguity function for the continuous signal model has been derived in [11, eqs. (48)–(50)].

The ambiguity function (3.6) has properties similar to the CRB. It decouples into a product of the *range-velocity ambiguity function* $\mathcal{A}(\boldsymbol{v}, \boldsymbol{v}_0)$ and the *DOA ambiguity function* $\mathcal{A}(\boldsymbol{\theta}, \boldsymbol{\theta}_0)$ (due to the space-time separability of signal and noise models), and there is a duality between the two ambiguity functions, like that between (3.1a) and (3.1c) in the CRB results (due to the symmetry in the signal and noise models).

It is easy to show that the CRB expressions in (3.1a) and (3.1c) are related to the DOA-range-velocity ambiguity function

$\mathcal{A}([\boldsymbol{\theta}^T,\boldsymbol{v}^T]^T,[\boldsymbol{\theta}_0^T,\boldsymbol{v}_0^T]^T)$ as

$$\mathrm{CRB}_{\theta\theta}|_{\boldsymbol{\theta}=\boldsymbol{\theta}_0,\boldsymbol{v}=\boldsymbol{v}_0} = -\frac{1}{\mathrm{SNR}}\cdot\left[\frac{\partial^2\mathcal{A}([\boldsymbol{\theta}^T,\boldsymbol{v}^T]^T,[\boldsymbol{\theta}_0^T,\boldsymbol{v}_0^T]^T)}{\partial\boldsymbol{\theta}\partial\boldsymbol{\theta}^T}\right]^{-1}\Bigg|_{\boldsymbol{\theta}=\boldsymbol{\theta}_0,\boldsymbol{v}=\boldsymbol{v}_0} \tag{3.8a}$$

$$\mathrm{CRB}_{\boldsymbol{vv}}|_{\boldsymbol{\theta}=\boldsymbol{\theta}_0,\boldsymbol{v}=\boldsymbol{v}_0} = -\frac{1}{\mathrm{SNR}}\cdot\left[\frac{\partial^2\mathcal{A}([\boldsymbol{\theta}^T,\boldsymbol{v}^T]^T,[\boldsymbol{\theta}_0^T,\boldsymbol{v}_0^T]^T)}{\partial\boldsymbol{v}\partial\boldsymbol{v}^T}\right]^{-1}\Bigg|_{\boldsymbol{\theta}=\boldsymbol{\theta}_0,\boldsymbol{v}=\boldsymbol{v}_0} \tag{3.8b}$$

It also holds that $[\partial\mathcal{A}(\boldsymbol{\theta},\boldsymbol{\theta}_0)/\partial\boldsymbol{\theta}^T]|_{\boldsymbol{\theta}=\boldsymbol{\theta}_0}=\mathbf{0}$ and $[\partial\mathcal{A}(\boldsymbol{v},\boldsymbol{v}_0)/\partial\boldsymbol{v}^T]|_{\boldsymbol{v}=\boldsymbol{v}_0}=\mathbf{0}$, and thus

$$\left[\frac{\partial^2\mathcal{A}([\boldsymbol{\theta}^T,\boldsymbol{v}^T]^T,[\boldsymbol{\theta}_0^T,\boldsymbol{v}_0^T]^T)}{\partial\boldsymbol{v}\partial\boldsymbol{\theta}^T}\right]\Bigg|_{\boldsymbol{\theta}=\boldsymbol{\theta}_0,\boldsymbol{v}=\boldsymbol{v}_0}=0 \tag{3.9}$$

which is equivalent to (3.1b). Therefore, the CRB for $\boldsymbol{\theta}$ and $\boldsymbol{v}$ in (3.1) is proportional to the inverse of the second derivative matrix of $\mathcal{A}([\boldsymbol{\theta}^T,\boldsymbol{v}^T]^T,[\boldsymbol{\theta}_0^T,\boldsymbol{v}_0^T]^T)$ with respect to $[\boldsymbol{\theta}^T,\boldsymbol{v}^T]^T$ evaluated at $[\boldsymbol{\theta}_0^T,\boldsymbol{v}_0^T]^T$. This is a well-known relationship between CRB and ambiguity function, which has been used in the analysis of both active and passive radar and sonar systems (see, e.g., [1, ch. 10, eqs. (96)–(98)] and [3, eq. (13)] for active radar systems and [14], [17, sec. V], and [18, sec. V] for passive arrays).

The CRB expressions (3.1) and (3.8) are heavily dependent on the temporal and spatial noise covariance matrices C and Σ, which (in the general case) precludes further interpretations and simplifications. Therefore, we will consider cases where the noise is temporally white (simplifying $\mathrm{CRB}_{\boldsymbol{vv}}$; see the following section) and spatially white (simplifying $\mathrm{CRB}_{\theta\theta}$; see Section IV).

C. CRB for Temporally White Noise

We now specialize the results of Section III-A to temporally white noise, i.e., $C=I_N$ (which is also the noise model used in [7] and [10]). Then, the expressions in (3.1a) and (3.1c) simplify to (A.11a) and (A.11b) in Appendix A2; see also [10].

The following assumption is useful to establish an analogy between the discrete-time (see above) and continuous-time processing of radar and sonar signals, the latter being widely used in the literature [1]–[3], [19]. Continuous-time results are often easier to interpret, at the cost of neglecting finite sampling effects. They also allow for time–frequency interpretations of the CRB.

Assumption A: The coherent processing interval of the received signal $\boldsymbol{\mu}[n,\boldsymbol{\gamma}]$ is completely covered by the observations $n=1,2,\cdots,N$ and the sampling is dense (i.e., $\Delta t\to 0$).

In the following, we derive the continuous CRB expressions for temporally white noise, i.e., noise having a flat power spectral density.

1) Continuous-time CRB with Flat Noise Power Spectral Density: Suppose Assumption A holds and that the power spectral density matrix $\mathcal{N}_\Sigma$ of the continuous-time noise $\boldsymbol{e}(t)$ is constant in the frequency band $f\in(-1/(2\Delta t),1/(2\Delta t))$, where f denotes the frequency in the continuous-time domain. (Then, the corresponding angular frequency is $\Omega=2\pi f$.) After Nyquist filtering and sampling, the noise $\boldsymbol{e}[n]$ is temporally white with spatial covariance $\Sigma=\mathcal{N}_\Sigma/\Delta t$. We define the vector of Doppler shift and time delay in the continuous-time domain as $\boldsymbol{\eta}=[\Omega_\mathrm{D},\tau]^T=[\omega_\mathrm{D}/\Delta t, n_\tau\cdot\Delta t]^T$. Denote by $S(\Omega)$ the Fourier transform of $s(t)$. Then, under Assumption A, the CRB expressions for $\boldsymbol{\theta}$ and $\boldsymbol{\eta}$ easily follow from (A.11) in Appendix A2:

$$\mathrm{CRB}_{\theta\theta}=\frac{\boldsymbol{a}(\boldsymbol{\theta})^*\mathcal{N}_\Sigma^{-1}\boldsymbol{a}(\boldsymbol{\theta})}{2\cdot\mathrm{SNR}}\cdot\left[\mathrm{Re}\left\{\frac{\partial\boldsymbol{a}(\boldsymbol{\theta})^*}{\partial\boldsymbol{\theta}}\mathcal{N}_\Sigma^{-1/2}\Pi_a^\perp(\boldsymbol{\theta},\mathcal{N}_\Sigma)\cdot\mathcal{N}_\Sigma^{-1/2}\frac{\partial\boldsymbol{a}(\boldsymbol{\theta})}{\partial\boldsymbol{\theta}^T}\right\}\right]^{-1} \tag{3.10a}$$

$$\mathrm{CRB}_{\boldsymbol{\eta\eta}}=\begin{bmatrix}\mathrm{CRB}_{\Omega_\mathrm{D}\Omega_\mathrm{D}} & \mathrm{CRB}_{\tau\Omega_\mathrm{D}}\\ \mathrm{CRB}_{\tau\Omega_\mathrm{D}} & \mathrm{CRB}_{\tau\tau}\end{bmatrix}=\frac{\varepsilon}{2\cdot\mathrm{SNR}}\cdot\begin{bmatrix}\delta & \mathrm{Imag}\{\xi\}\\ \mathrm{Imag}\{\xi\} & \beta\end{bmatrix}^{-1} \tag{3.10b}$$

where

$$\varepsilon=\int_{-\infty}^{\infty}|s(t-\tau)|^2\,dt=\int_{-\infty}^{\infty}|S(\Omega)|^2\,df \tag{3.11a}$$

$$\delta=\int_{-\infty}^{\infty}t^2|s(t-\tau)|^2\,dt-\frac{1}{\varepsilon}\cdot\left[\int_{-\infty}^{\infty}t|s(t-\tau)|^2\,dt\right]^2 \tag{3.11b}$$

$$\xi=\int_{-\infty}^{\infty}ts(t-\tau)\frac{ds(t-\tau)^*}{dt}dt-\frac{1}{\varepsilon}\cdot\int_{-\infty}^{\infty}t|s(t-\tau)|^2\,dt\cdot\int_{-\infty}^{\infty}s(t-\tau)\frac{ds(t-\tau)^*}{dt}dt \tag{3.11c}$$

$$\beta=\int_{-\infty}^{\infty}\left|\frac{ds(t-\tau)}{dt}\right|^2dt-\frac{1}{\varepsilon}\left|\int_{-\infty}^{\infty}s(t-\tau)\frac{ds(t-\tau)^*}{dt}dt\right|^2 \tag{3.11d}$$

$$=\int_{-\infty}^{\infty}\Omega^2|S(\Omega)|^2\,df-\frac{1}{\varepsilon}\cdot\left|\int_{-\infty}^{\infty}\Omega|S(\Omega)|^2\,df\right|^2 \tag{3.11e}$$

$$\mathrm{SNR}=|x|^2\cdot\int_{-\infty}^{\infty}|s(t-\tau)|^2\,dt\cdot\boldsymbol{a}(\boldsymbol{\theta})^*\mathcal{N}_\Sigma^{-1}\boldsymbol{a}(\boldsymbol{\theta})=|x|^2\cdot\varepsilon\cdot\boldsymbol{a}(\boldsymbol{\theta})^*\mathcal{N}_\Sigma^{-1}\boldsymbol{a}(\boldsymbol{\theta}) \tag{3.11f}$$

which follow from (A.10) and (A.12). Here, ε, δ/ε, and β/ε become proportional to the signal energy, square of the root mean square (rms) duration, and the square of rms bandwidth of $s(t)$, respectively [10] (see also [20, Sec. 1.2 and 1.3], where the signal energy is normalized, i.e., $\varepsilon=1$). It is easy to show that the expressions in (3.11) are invariant to translation in time and therefore do not depend on the time delay; see also [10]. As a result, the expressions in (3.11) remain valid if we replace τ with 0.

To find the time–frequency interpretation of ξ, we need to use the following representation of the complex envelope: $s(t)=u(t)\exp[j\varpi(t)]$, where $u(t)$ and $\varpi(t)$ are the magnitude and phase, respectively. Define the instantaneous

frequency of the complex envelope as $\Omega_{\mathrm{i}}(t) = d\varpi(t)/dt$. Then, $ds(t)/dt = du(t)/dt \cdot \exp[j\varpi(t)] + ju(t)\Omega_{\mathrm{i}}(t) \exp[j\varpi(t)]$, and

$$-\frac{\mathrm{Imag}\{\xi\}}{\varepsilon} = \frac{\int_{-\infty}^{\infty} t\Omega_{\mathrm{i}}(t)u(t)^2\,dt}{\int_{\infty}^{\infty} u(t)^2\,dt} - \frac{\int_{\infty}^{\infty} tu(t)^2\,dt}{\int_{\infty}^{\infty} u(t)^2\,dt} \cdot \frac{\int_{-\infty}^{\infty} \Omega_{\mathrm{i}}(t)u(t)^2\,dt}{\int_{\infty}^{\infty} u(t)^2\,dt} \tag{3.12}$$

which can be viewed as the "covariance" of a signal, i.e., the measure of how time is correlated with instantaneous frequency. Indeed, for normalized signal energy, it equals the signal covariance expression in [20, eq. (1.124)].

For flat noise power spectral density and under Assumption A, the range-velocity ambiguity function in (3.7a) simplifies to

$$\mathcal{A}(\boldsymbol{\eta}, \boldsymbol{\eta}_0) = \mathcal{A}(\boldsymbol{\eta} - \boldsymbol{\eta}_0) = \frac{1}{\left|\int_{-\infty}^{\infty} |s(t)|^2\,dt\right|^2} \cdot \left|\int_{-\infty}^{\infty} s\left(t - \frac{\tilde{\tau}}{2}\right) s\left(t + \frac{\tilde{\tau}}{2}\right)^* \exp(j\tilde{\Omega}_{\mathrm{D}} t)\,dt\right|^2 \tag{3.13}$$

where $\tilde{\tau} = \tau - \tau_0$ and $\tilde{\Omega}_{\mathrm{D}} = \Omega_{\mathrm{D}} - \Omega_{\mathrm{D0}}$. Here, $\boldsymbol{\eta} = [\Omega_{\mathrm{D}}, \tau]^T$ and $\boldsymbol{\eta}_0 = [\Omega_{\mathrm{D0}}, \tau_0]^T$ are the vectors of Doppler shifts and time delays in the continuous domain for the two targets. Note that the ambiguity function in (3.13) is equal to the (normalized) Woodward's ambiguity function for a single antenna in, for example, [1, p. 279]. It follows from (3.6) and (3.8b) that the $\mathrm{CRB}_{\boldsymbol{\eta}\boldsymbol{\eta}}$ for $\boldsymbol{\eta} = \boldsymbol{\eta}_0$ is proportional to the inverse of the second derivative matrix of this ambiguity function with respect to $\boldsymbol{\eta} - \boldsymbol{\eta}_0 = [\tilde{\Omega}_{\mathrm{D}}, \tilde{\tau}]^T$ evaluated at $\tilde{\Omega}_{\mathrm{D}} = 0$, $\tilde{\tau} = 0$.

Observe that the CRB results in (3.10) do not depend on the sampling interval Δt because, under the above noise model, the noise level increases as Δt decreases (since $\Sigma = \mathcal{N}_\Sigma/\Delta t$), cancelling out the linear decrease of the CRB due to the oversampling.

In the following section, we apply equations (3.10) and (3.11) to compute the approximate CRB expressions for the time delay τ, Doppler shift Ω_{D}, and direction $\boldsymbol{\theta}$ for the practically important case where $s(t)$ is a sequence of rectangular chirp pulses with large time-bandwidth product.

2) Continuous-time CRB for Rectangular Chirp Pulses in Temporally White Noise: In this section, we assume that Assumption A holds, the noise has flat power spectral density (as in Section III-C.1), and $s(t)$ consists of P rectangular chirp pulses

$$s(t) = \sum_{p=0}^{P-1} s_0(t - pT_{\mathrm{R}}) \tag{3.14}$$

where T_{R} is the pulse repetition interval, and a single chirp pulse (see, e.g., [21, sec. V] and [22, ch. 6.6]) is

$$s_0(t) = \exp\left[j\pi \frac{f_{\mathrm{B}}}{T_0}\left(t - \frac{1}{2}T_0\right)^2\right] \cdot [h(t) - h(t - T_0)] \tag{3.15}$$

where

- T_0 single pulse duration;
- f_{B} bandwidth of the chirp pulse (in the continuous domain);
- $h(t)$ Heaviside step function.

Properties of a rectangular chirp signal and its spectrum have been studied extensively in radar and sonar literature [1, p. 292], [2, ch. 6.3], [19, ch. 6.3 and 7], [21, sec. V], [22, ch. 6.6].

Assume that the time-bandwidth product of a pulse is large, i.e., $T_0 f_{\mathrm{B}} \gg 1$. Then, an approximate CRB for $\boldsymbol{\eta}$ is (see Appendix C)

$$\mathrm{CRB}_{\boldsymbol{\eta}\boldsymbol{\eta}} = \frac{1}{2 \cdot P \cdot \mathrm{SNR}_1} \cdot \begin{bmatrix} \frac{1}{12}(T_0)^2 \cdot \left[1 + \left(\frac{T_{\mathrm{R}}}{T_0}\right)^2 (P^2 - 1)\right] & -\frac{1}{6}\pi f_{\mathrm{B}} T_0 \\ -\frac{1}{6}\pi f_{\mathrm{B}} T_0 & \frac{1}{3}\pi^2 f_{\mathrm{B}}^2 \end{bmatrix}^{-1} \tag{3.16}$$

where

$$\mathrm{SNR}_1 = |x|^2 \cdot T_0 \cdot \boldsymbol{a}(\boldsymbol{\theta})^* \mathcal{N}_\Sigma^{-1} \boldsymbol{a}(\boldsymbol{\theta}) \tag{3.17}$$

is the SNR for a single pulse. The large time-bandwidth assumption allows us to approximate the spectrum of a chirp pulse by a rectangular distribution, which is needed to compute the rms bandwidth term in (3.16); see Appendix C. The expression for $\mathrm{CRB}_{\theta\theta}$ is the same as in (3.10a), where SNR is replaced with $P \cdot \mathrm{SNR}_1$.

For only one pulse (i.e., $P = 1$), the CRB in (3.16) goes to infinity since the model is not identifiable. The identifiability problem appears because the time delay and Doppler shift cannot be uniquely estimated, which can be explained by considering a single pulse received by one sensor. The signal received by the sensor is proportional to

$$\begin{aligned} s_0(t - \tau)\exp(j\Omega_{\mathrm{D}} t) &= \exp\left(j\pi \frac{f_{\mathrm{B}}}{T_0}\left(t - \tau - \frac{1}{2}T_0\right)^2 + j\Omega_{\mathrm{D}} t\right) \\ &= \exp\left[j\pi \frac{f_{\mathrm{B}}}{T_0} t^2\right] \cdot \exp\left(j\pi \frac{f_{\mathrm{B}}}{T_0}\left(\tau + \frac{1}{2}T_0\right)^2\right) \\ &\quad \cdot \exp\left(j\left[\Omega_{\mathrm{D}} - \frac{2\pi f_{\mathrm{B}}}{T_0}\left(\tau + \frac{1}{2}T_0\right)\right] t\right) \\ &\quad 0 < t - \tau < T_0. \end{aligned} \tag{3.18}$$

The first factor in (3.18) is independent of $\boldsymbol{\eta}$, and the second term, which does not depend on t, can be absorbed into the unknown complex amplitude x. Therefore, only the third term can be used to estimate $\boldsymbol{\eta}$. However, τ and Ω_{D} are coupled in the

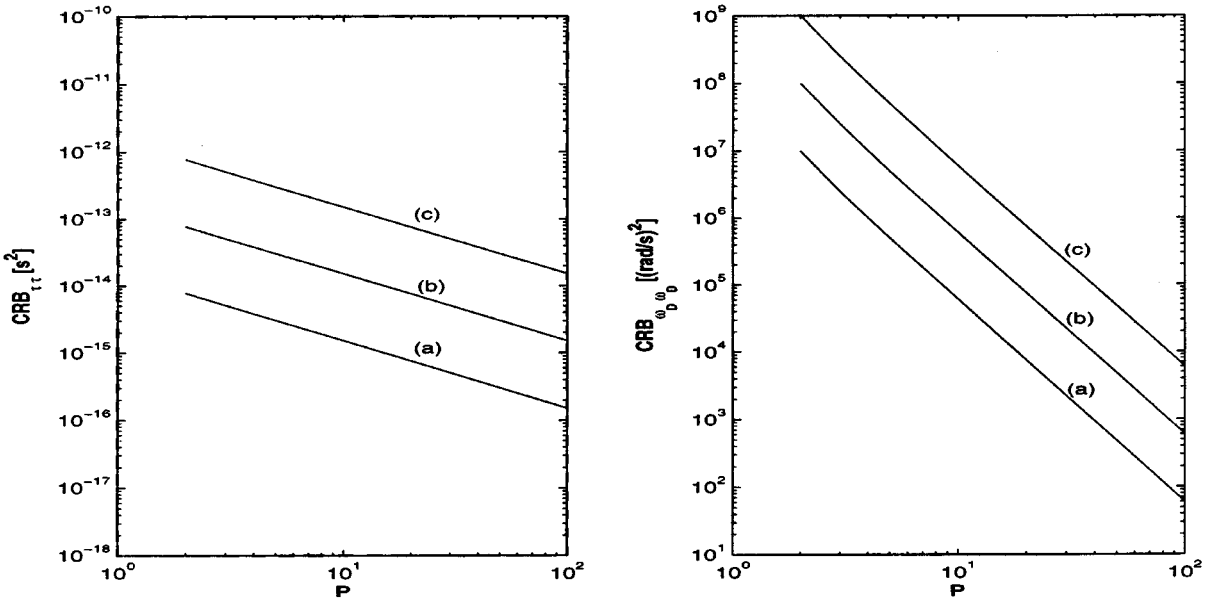

Fig. 2. CRB on (left) time delay τ and (right) Doppler shift $\Omega_{\rm D}$ for a sequence of rectangular chirp pulses with bandwidth $f_{\rm B} = 10$ MHz, repetition period $T_{\rm R} = 1$ ms, and pulse duration $T_0 = 250\,\mu$s as a function of the number of pulses P. (a) $\text{SNR}_1 = -10$ dB. (b) $\text{SNR}_1 = -20$ dB. (c) $\text{SNR}_1 = -30$ dB, where SNR_1 is the SNR for one pulse.

third term and cannot be uniquely estimated (only their linear combination $\Omega_{\rm D} - 2\pi f_{\rm B}\tau/T_0$ can be estimated).

Inverting $\text{CRB}_{\boldsymbol{\eta\eta}}$ in (3.16) yields the following CRB expressions for $\Omega_{\rm D}$ and τ:

$$\text{CRB}_{\tau\tau} = \frac{3}{2\pi^2 f_{\rm B}^2 \cdot \text{SNR}_1} \cdot \frac{1}{P} \cdot \left[1 + \frac{1}{P^2-1} \cdot \left(\frac{T_0}{T_{\rm R}}\right)^2\right] \quad (3.19a)$$

$$\text{CRB}_{\Omega_{\rm D}\Omega_{\rm D}} = \frac{6}{\text{SNR}_1 \cdot T_{\rm R}^2} \cdot \frac{1}{P(P^2-1)}. \quad (3.19b)$$

If the repetition period $T_{\rm R}$ and single pulse duration T_0 are fixed, then $\text{CRB}_{\Omega_{\rm D}\Omega_{\rm D}}$ decreases with the third power of P for large P. However, the number of pulses is limited by the duration of the coherence interval $T_{\rm CPI}$. If the coherence time and relative single pulse duration with respect to the repetition period are fixed (i.e., $T_{\rm CPI} = PT_{\rm R} = \text{const}$ and $T_0/T_{\rm R} = \text{const}$), then $\text{CRB}_{\Omega_{\rm D}\Omega_{\rm D}}$ will be independent of P for large P [observe that SNR_1 is proportional to T_0; see (3.17)].

If the bandwidth $f_{\rm B}$ and single pulse duration T_0 are fixed, then $\text{CRB}_{\tau\tau}$ decreases linearly with the number of pulses P for large P. If the coherence time and relative single pulse duration with respect to the repetition period are again fixed (in addition to bandwidth), $\text{CRB}_{\tau\tau}$ will be independent of P for large P.

Finally, for fixed $T_{\rm R}$ and T_0, $\text{CRB}_{\boldsymbol{\eta\eta}}$ in (3.16) decouples as P increases, i.e., $\text{CRB}_{\Omega_{\rm D}\Omega_{\rm D}}$ becomes approximately the same, regardless of whether or not τ is known, and similarly, $\text{CRB}_{\tau\tau}$ becomes the same, regardless of whether or not $\Omega_{\rm D}$ is known. This result follows from the fact that $\delta\cdot\beta - \text{Imag}\{\xi\}^2 \approx \delta\cdot\beta$ for large P [since, for large P, $\delta\cdot\beta$ becomes proportional to P^4, whereas $\text{Imag}\{\xi\}^2$ is proportional to P^2; see (C.1b) and (C.2) in Appendix C].

3) Radar Numerical Example: In Fig. 2, we plot the CRBs for time delay τ and Doppler shift $\Omega_{\rm D}$ in (3.19a) and (3.19b) as a function of the number of pulses P and SNR_1 (i.e., the SNR for one pulse). We have chosen the following chirp signal parameters:

- carrier frequency $f_{\rm c} = 10$ GHz;
- bandwidth $f_{\rm B} = 10$ MHz;
- repetition period $T_{\rm R} = 1$ ms;
- pulse duration $T_0 = T_{\rm R}/4 = 250\,\mu$s.

For these parameters, the approximate expressions in (3.19) are valid since the time-bandwidth product of the pulse is large: $T_0 f_{\rm B} = 2500 \gg 1$. Note that for $\text{SNR} = P\cdot\text{SNR}_1 = 1$ (i.e., 0 dB), we have $\text{CRB}_{\tau\tau} = 15.2\cdot 10^{-16}$ s^2, and the corresponding CRB for the range is then (5.85 m)^2 (since the range $\rho = \tau c/2$). For $\text{SNR}_1 = 0.01$ (i.e., -20 dB) and $P = 100$ (thus SNR $= P\cdot\text{SNR}_1 = 1 = 0$ dB), we have $\text{CRB}_{\omega_{\rm D}\omega_{\rm D}} = 600$ (rad/s)^2, and the corresponding CRB for velocity is then (5.85 cm/s)^2 (since $v = \Omega_{\rm D}c/(2\Omega_{\rm c})$, and $\Omega_{\rm c} = 2\pi f_{\rm c}$).

IV. CRB for Arrays of Identical Isotropic Sensors in Spatially White Noise

In this section, we derive CRB expressions for an array of identical isotropic sensors and spatially white noise. We also discuss the case when the noise is both spatially and temporally white. In Section IV-A, we compute the volume of the confidence region for the target's location, which we propose as a measure of estimation accuracy for the target's location.

A sensor array consisting of identical isotropic sensors has an array response vector of the form $\boldsymbol{a}(\boldsymbol{\theta}) = [\exp(j\Omega_{\rm c}\tau_1(\boldsymbol{\theta})), \cdots, \exp(j\Omega_{\rm c}\tau_m(\boldsymbol{\theta}))]^T$, where $\tau_k(\boldsymbol{\theta}), k = 1,\cdots,m$ are the differential time delays between the sensors. A spatially white noise assumption implies that $\Sigma = \sigma^2\cdot I_m$. Based on the above assumptions $\boldsymbol{a}(\boldsymbol{\theta})^*\Sigma^{-1}\boldsymbol{a}(\boldsymbol{\theta}) = m/\sigma^2$, and the SNR in (3.5)

simplifies to $\text{SNR} = |x|^2 \cdot \boldsymbol{\phi}(\boldsymbol{v})^* C^{-1} \boldsymbol{\phi}(\boldsymbol{v}) \cdot m/\sigma^2$, whereas $\text{CRB}_{\theta\theta}$ in (3.1a) becomes

$$\begin{aligned}\text{CRB}_{\theta\theta} &= \frac{m}{2 \cdot \text{SNR}} \left[\text{Re} \left\{ \frac{\partial \boldsymbol{a}(\boldsymbol{\theta})^*}{\partial \boldsymbol{\theta}} \right. \right. \\ &\quad \left. \left. \cdot \left[I_m - \frac{\boldsymbol{a}(\boldsymbol{\theta}) \boldsymbol{a}(\boldsymbol{\theta})^*}{\boldsymbol{a}(\boldsymbol{\theta})^* \boldsymbol{a}(\boldsymbol{\theta})} \right] \cdot \frac{\partial \boldsymbol{a}(\boldsymbol{\theta})}{\partial \boldsymbol{\theta}^T} \right\} \right]^{-1} \\ &= \frac{m}{2\Omega_c^2 \cdot \text{SNR}} \cdot W(\boldsymbol{\theta})^{-1} \end{aligned} \tag{4.1}$$

where

$$\begin{aligned} W(\boldsymbol{\theta}) &= \sum_{k=1}^{m} \left(\frac{d\tau_k(\boldsymbol{\theta})}{d\boldsymbol{\theta}} - \frac{d\overline{\tau}(\boldsymbol{\theta})}{d\boldsymbol{\theta}} \right) \cdot \left(\frac{d\tau_k(\boldsymbol{\theta})}{d\boldsymbol{\theta}} - \frac{d\overline{\tau}(\boldsymbol{\theta})}{d\boldsymbol{\theta}} \right)^T \\ &= \begin{bmatrix} W_{11} & W_{12} \\ W_{12} & W_{22} \end{bmatrix} \end{aligned} \tag{4.2a}$$

$$\overline{\tau}(\boldsymbol{\theta}) = \frac{1}{m} \sum_{k=1}^{m} \tau_k(\boldsymbol{\theta}). \tag{4.2b}$$

Here, $\overline{\tau}(\boldsymbol{\theta})$ is the average differential time delay for the whole array, and $W(\boldsymbol{\theta})$ is the array spreading matrix of the derivatives of the differential delays with respect to the DOA parameters $\boldsymbol{\theta}$. The entries W_{11}, W_{12}, and W_{22} of $W(\boldsymbol{\theta})$ are functions of $\boldsymbol{\theta}$, but we have omitted this dependence for notational simplicity.

If, in addition, the noise is temporally white (i.e., $C = I_N$), the expression $\text{CRB}_{\theta\theta}$ in (4.1) holds, with the SNR simplifying to $\text{SNR} = |x|^2 \cdot \sum_{n=1}^{N} |s[n - n_\tau]|^2 \cdot m/\sigma^2$; see Section III-C . If Assumption A holds and the noise is both spatially and temporally white, i.e., $\mathcal{N}_\Sigma = n_\Sigma \cdot I_m$ (see also Section III-C1), the SNR further becomes $\text{SNR} = |x|^2 \cdot \int_{-\infty}^{\infty} |s(t)|^2 \, dt \cdot m/n_\Sigma$. Then, from (3.10b), it follows that the accuracies of the Doppler shift and time delay estimation do not depend on the array configuration. In addition, $\text{CRB}_{\boldsymbol{\eta}\boldsymbol{\eta}}$ is proportional to $1/m$; thus, it can be achieved asymptotically by merely averaging the single-sensor ML estimates of $\boldsymbol{\eta}$ over all sensors.

For spatially white noise, the DOA ambiguity function in (3.7b) simplifies to

$$\mathcal{A}(\boldsymbol{\theta}, \boldsymbol{\theta}_0) = \frac{1}{m^2} \cdot \left| \sum_{k=1}^{m} \exp\{ j\Omega_c [\tau_k(\boldsymbol{\theta}) - \tau_k(\boldsymbol{\theta}_0)] \} \right|^2. \tag{4.3}$$

It follows from (3.6) and (3.8a) that $\text{CRB}_{\theta\theta}$ for $\boldsymbol{\theta} = \boldsymbol{\theta}_0$ is proportional to the inverse of the second derivative matrix of the above ambiguity function with respect to $\boldsymbol{\theta}$, evaluated at $\boldsymbol{\theta}_0$.

Consider now a simple case of isotropic sensors distributed in 3-D to measure an incoming plane wave characterized by the vector of DOA parameters $\boldsymbol{\theta} = [\phi, \psi]^T$, where ϕ and ψ are azimuth and elevation, respectively. The kth sensor is located at (x_k, y_k, z_k) for $k = 1, 2, \cdots, m$. Then, $\tau_k(\boldsymbol{\theta}) = (x_k \cos\phi \cos\psi + y_k \sin\phi \cos\psi + z_k \sin\psi)/c$; see, for instance, [23] and [24]. Further

$$\begin{aligned} \frac{d\tau_k(\boldsymbol{\theta})}{d\boldsymbol{\theta}^T} &= \frac{1}{c} [(-x_k \sin\phi + y_k \cos\phi) \cdot \cos\psi, -x_k \cos\phi \\ &\quad \cdot \sin\psi - y_k \sin\phi \sin\psi + z_k \cos\psi] \end{aligned} \tag{4.4}$$

and the elements of $W(\boldsymbol{\theta})$ are

$$\begin{aligned} W_{11} &= \frac{\cos^2\psi}{c^2} \sum_{k=1}^{m} [-(x_k - \overline{x}) \sin\phi + (y_k - \overline{y}) \cos\phi]^2 \\ &= \frac{\cos^2\psi}{c^2} (Q_{xx} \sin^2\phi + Q_{yy} \cos^2\phi - Q_{xy} \sin 2\phi) \end{aligned} \tag{4.5a}$$

$$\begin{aligned} W_{12} &= \frac{\cos\psi}{c^2} \cdot \sum_{k=1}^{m} [-(x_k - \overline{x}) \sin\phi + (y_k - \overline{y}) \cos\phi] \\ &\quad \cdot [-(x_k - \overline{x}) \cos\phi \sin\psi - (y_k - \overline{y}) \sin\phi \\ &\quad \cdot \sin\psi + (z_k - \overline{z}) \cos\psi] \\ &= \frac{\cos\psi}{c^2} \cdot \left\{ \left[\frac{1}{2} (Q_{xx} - Q_{yy}) \sin 2\phi - Q_{xy} \cos 2\phi \right] \right. \\ &\quad \left. \cdot \sin\psi + (Q_{yz} \cos\phi - Q_{xz} \sin\phi) \cos\psi \right\} \end{aligned} \tag{4.5b}$$

$$\begin{aligned} W_{22} &= \frac{1}{c^2} \cdot \sum_{k=1}^{m} [-(x_k - \overline{x}) \cos\phi \sin\psi - (y_k - \overline{y}) \\ &\quad \cdot \sin\phi \sin\psi + (z_k - \overline{z}) \cos\psi]^2 \\ &= \frac{1}{c^2} \cdot \{ (Q_{xx} \cos^2\phi + Q_{yy} \sin^2\phi) \sin^2\psi \\ &\quad + Q_{zz} \cos^2\psi + Q_{xy} \sin 2\phi \sin^2\psi \\ &\quad - (Q_{xz} \cos\phi + Q_{yz} \sin\phi) \sin 2\psi \} \end{aligned} \tag{4.5c}$$

$$\overline{x} = \frac{1}{m} \sum_{k=1}^{m} x_k, \quad \overline{y} = \frac{1}{m} \sum_{k=1}^{m} y_k, \quad \overline{z} = \frac{1}{m} \sum_{k=1}^{m} z_k \tag{4.5d}$$

$$\begin{aligned} Q_{xx} &= \sum_{k=1}^{m} (x_k - \overline{x})^2, \quad Q_{yy} = \sum_{k=1}^{m} (y_k - \overline{y})^2 \\ Q_{zz} &= \sum_{k=1}^{m} (z_k - \overline{z})^2, \quad Q_{xy} = \sum_{k=1}^{m} (x_k - \overline{x})(y_k - \overline{y}) \\ Q_{xz} &= \sum_{k=1}^{m} (x_k - \overline{x})(z_k - \overline{z}), \quad Q_{yz} = \sum_{k=1}^{m} (y_k - \overline{y})(z_k - \overline{z}). \end{aligned} \tag{4.5e}$$

In (4.5d) and (4.5e), we have introduced $\overline{x}$, $\overline{y}$, and $\overline{z}$ describing the *center of gravity*, or *phase center*, of the array [25, p. 113]] and the array configuration parameters Q_{xx}, Q_{xy}, Q_{xz}, Q_{yy}, Q_{yz}, and Q_{zz}, describing the *moment-of-inertia tensor* of the array; see [26, ch. 6]. Here, we assume that each sensor is associated with a unit "mass."

Therefore, for an array of isotropic sensors receiving a reflected plane wave corrupted by spatially white noise, $\text{CRB}_{\theta\theta}$ depends on the array geometry only through the above moment-of-inertia parameters, whereas $\text{CRB}_{\boldsymbol{v}\boldsymbol{v}}$ is independent of the array geometry [which easily follows from (3.1c) and the fact that $\boldsymbol{a}(\boldsymbol{\theta})^* \Sigma^{-1} \boldsymbol{a}(\boldsymbol{\theta}) = m/\sigma^2$].

For a large number of sensors (i.e., $m \to \infty$) uniformly distributed over a certain volume $\mathcal{V}$, the summations in the above expressions can be replaced by integrals over $\mathcal{V}$, which simplifies the computation. This case is of practical interest since modern radar arrays contain hundreds of antennas; see, for example, [27]. Assume, without loss of generality, that the center

of the coordinate system is located at the phase center, i.e., at $\overline{x} = \overline{y} = \overline{z} = 0$. Then

$$Q_{xx} = \frac{m}{V} \cdot \int_{\mathcal{V}} x^2 \, dx \, dy \, dz \tag{4.6a}$$

$$Q_{xy} = \frac{m}{V} \cdot \int_{\mathcal{V}} xy \, dx \, dy \, dz \tag{4.6b}$$

$$V = \int_{\mathcal{V}} dx \, dy \, dz \tag{4.6c}$$

and the expressions for Q_{yy}, Q_{zz}, Q_{xz}, and Q_{yz} follow by analogy.

A. Volume of the Confidence Region for the Target's Location

We compute the volume of the (linearized) confidence region for the target's location expressed in Cartesian coordinates. This volume is a measure of location performance that can be achieved using given array geometry and signal waveform. Similar performance measures have been used in [18, sec. V] and [28]. We assume that Assumption A holds and that the noise is both spatially and temporally white, i.e., $\mathcal{N}_\Sigma = n_\Sigma \cdot I_m$. We show that this volume is minimized and maximized for targets lying along the principal axes of inertia of the array. We will find conditions for this volume to be independent of the azimuth ϕ. For this azimuth-invariant case, we will then show the dependence of the confidence volume on the array configuration (through the moment-of-inertia parameters) and target's elevation angle ψ. Finally, we will compare these volumes for several 3-D array configurations that are azimuth invariant.

Define the vector of target location parameters in the Cartesian coordinate system $\boldsymbol{\zeta} = [x_{\mathrm{T}}, y_{\mathrm{T}}, z_{\mathrm{T}}]^T$ and in the spherical coordinate system $\boldsymbol{\alpha} = [\tau, \phi, \psi]^T$. Then, the transformation from spherical to Cartesian coordinates (see Fig. 3) is

$$x_{\mathrm{T}} = \tfrac{1}{2} c\tau \cos\phi \cos\psi \tag{4.7a}$$

$$y_{\mathrm{T}} = \tfrac{1}{2} c\tau \sin\phi \cos\psi \tag{4.7b}$$

$$z_{\mathrm{T}} = \tfrac{1}{2} c\tau \sin\psi \tag{4.7c}$$

yielding

$$\frac{\partial \boldsymbol{\zeta}}{\partial \boldsymbol{\alpha}^T} = \begin{bmatrix} \frac{1}{2}c\cos\phi\cos\psi & -\frac{1}{2}c\tau\sin\phi\cos\psi & -\frac{1}{2}c\tau\cos\phi\sin\psi \\ \frac{1}{2}c\sin\phi\cos\psi & \frac{1}{2}c\tau\cos\phi\cos\psi & -\frac{1}{2}c\tau\sin\phi\sin\psi \\ \frac{1}{2}c\sin\psi & 0 & \frac{1}{2}c\tau\cos\psi \end{bmatrix}. \tag{4.8}$$

Let V_ζ be the volume of the linearized confidence region (which is an ellipsoid) for the target's location $\boldsymbol{\zeta}$. Then, ${V_\zeta}^2$ is proportional to $|\mathrm{CRB}_{\boldsymbol{\zeta\zeta}}|$ (where $|\cdot|$ denotes the determinant), as shown in Appendix D, and

$$\begin{aligned} {V_\zeta}^2 \sim |\mathrm{CRB}_{\boldsymbol{\zeta\zeta}}| &= \left| \frac{\partial \boldsymbol{\zeta}}{\partial \boldsymbol{\alpha}^T} \mathrm{CRB}_{\boldsymbol{\alpha\alpha}} \frac{\partial \boldsymbol{\zeta}^T}{\partial \boldsymbol{\alpha}} \right| \\ &= \left| \frac{\partial \boldsymbol{\zeta}}{\partial \boldsymbol{\alpha}^T} \right|^2 \cdot |\mathrm{CRB}_{\boldsymbol{\alpha\alpha}}| \\ &= \left| \frac{\partial \boldsymbol{\zeta}}{\partial \boldsymbol{\alpha}^T} \right|^2 \cdot \mathrm{CRB}_{\tau\tau} \cdot |\mathrm{CRB}_{\theta\theta}|. \end{aligned} \tag{4.9}$$

The last equality follows from $\mathrm{CRB}_{\boldsymbol{\theta\theta}} = 0$, and therefore, $\mathrm{CRB}_{\tau\boldsymbol{\theta}} = 0$. Observe that $\mathrm{CRB}_{\tau\tau}$ does not depend on the target's location [which follows from $\boldsymbol{a}(\boldsymbol{\theta})^* \mathcal{N}_\Sigma^{-1} \boldsymbol{a}(\boldsymbol{\theta}) = m/n_\Sigma$ (3.10b) and the fact that the expressions in (3.11) do not depend on τ]. At first, this result may seem unrealistic since, intuitively, we expect $\mathrm{CRB}_{\tau\tau}$ to increase with the range of the target. However, it holds for the model that we adopted in Section II, where the complex amplitude x is assumed to be an unknown deterministic constant. In reality, x is a function of range ρ (i.e., $|x|$ is approximately related to the target's range as $|x| \sim \rho^{-2} \sim \tau^{-2}$), as well as a variety of other target-specific parameters (e.g., target's shape, orientation, material; see [22, ch. 3]). [Note that incorporating the dependence $|x| \sim \rho^{-2}$ in (3.10b) yields $\mathrm{CRB}_{\tau\tau} \sim \rho^4 \sim \tau^4$, which is intuitively appealing.] In addition, from (4.8) and (4.1), we have

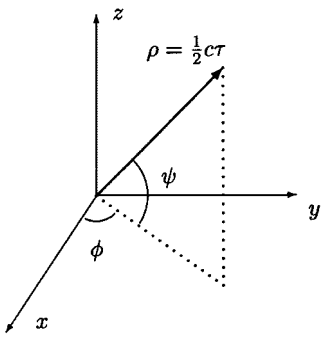

Fig. 3. Target coordinates in a spherical coordinate system.

$$\left| \frac{\partial \boldsymbol{\zeta}}{\partial \boldsymbol{\alpha}^T} \right| = \frac{c^3 \tau^2}{8} \cos\psi \tag{4.10a}$$

$$|\mathrm{CRB}_{\theta\theta}| = \left(\frac{m}{2\Omega_{\mathrm{c}}^2 \cdot \mathrm{SNR}} \right)^2 \cdot \frac{1}{W_{11}W_{22} - {W_{12}}^2} \tag{4.10b}$$

which, together with (3.10b) and (3.11f), implies that the volume of the confidence ellipsoid for the target location vector $\boldsymbol{\zeta}$ depends on the target's location as follows:

$$V_\zeta \sim \frac{1}{|x|^3} \cdot \frac{\tau^2 \cdot |\cos\psi|}{\sqrt{W_{11}W_{22} - {W_{12}}^2}}. \tag{4.11}$$

Observe that V_ζ depends on the direction parameters $\boldsymbol{\theta}$ only through the elements of the array spreading matrix $W(\boldsymbol{\theta})$ in (4.5) and a $\cos\psi$ factor in the numerator, which cancels out the artificial singularity in the denominator inherent to the spherical coordinate system. This singularity appears because the azimuth ϕ is not identifiable if $|\psi| = \pi/2$. For $|\psi| = \pi/2$, the volume of the confidence ellipsoid for the target location vector $\boldsymbol{\alpha}$ (in spherical coordinates) would go to infinity; however, it is finite for $\boldsymbol{\zeta}$ (i.e., the target's location in Cartesian coordinates).

Without loss of generality, we choose the x, y, and z axes of the Cartesian coordinate system to coincide with the *principal axes of inertia* [26, ch. 6] of the array, implying that $Q_{xy} = Q_{xz} = Q_{yz} = 0$. In addition, we choose the center of the coordinate system to coincide with the phase center, i.e., $\overline{x} = \overline{y} = \overline{z} = 0$. Then, we show in Appendix E that we have

$$V_\zeta \sim \frac{(x_{\mathrm{T}}^2 + y_{\mathrm{T}}^2 + z_{\mathrm{T}}^2)^{3/2}}{|x|^3 \cdot \sqrt{Q_{zz}Q_{xx} \cdot y_{\mathrm{T}}^2 + Q_{yy}Q_{zz} \cdot x_{\mathrm{T}}^2 + Q_{xx}Q_{yy} \cdot z_{\mathrm{T}}^2}} \tag{4.12}$$

which is minimized (under a fixed range constraint, i.e., $\rho = c\tau/2 = (x_{\mathrm{T}}^2 + y_{\mathrm{T}}^2 + z_{\mathrm{T}}^2)^{1/2} = \text{const}$) if the target lies on one of the principal axes of inertia. Assume, without loss of generality, that this axis is the z-axis; then, it holds that $Q_{xx}Q_{yy} = \max\{Q_{xx}Q_{yy}, Q_{yy}Q_{zz}, Q_{zz}Q_{xx}\}$; see Appendix E. This result means that the most desirable DOA in terms of the volume of the target location confidence ellipsoid is along the z axis or, equivalently, for the elevation $|\psi| = \pi/2$. In addition, note that the least desirable DOA in terms of target location accuracy would then be along the x or y axes (or both); see Appendix E. Therefore, for an array of identical isotropic sensors in both spatially and temporally white noise, it follows that the most and the least desirable DOAs (in terms of the volume of the confidence ellipsoid) are always perpendicular to each other. For example, for a *planar array* lying in the x-y plane, the most desirable DOA, which defines the z axis, is perpendicular to the array. This easily follows from the fact that $Q_{zz} = 0$. The expression (4.12) goes to infinity for targets lying in the x-y plane (i.e., when $z_{\mathrm{T}} = 0$), which defines the set of the least desirable DOAs.

It is of practical interest to consider the case where the confidence volume V_ζ does not depend on the azimuth ϕ. From (4.12) and (E.2a) in Appendix E, it follows that this condition is satisfied if $Q_{xx} = Q_{yy} = Q$. The conditions $Q_{xy} = Q_{xz} = Q_{yz} = 0$ and $Q_{xx} = Q_{yy}$ were shown in [23] to be necessary and sufficient for $\mathrm{CRB}_{\theta\theta}$ to be block-diagonal; see, in addition, [24]. In our case, $Q_{xy} = Q_{xz} = Q_{yz} = 0$ follows due to the choice of the principal axes of inertia to be the x, y, and z axes, whereas $Q_{xx} = Q_{yy}$ is needed to ensure an azimuth-invariant performance of the array. Under both of the above conditions, the expressions in (4.5) simplify to

$$W_{11} = \frac{\cos^2\psi}{c^2}Q \tag{4.13a}$$

$$W_{12} = 0 \tag{4.13b}$$

$$W_{22} = \frac{1}{c^2}[Q\sin^2\psi + Q_{zz}\cos^2\psi] \tag{4.13c}$$

which, also using (4.1) and (4.11), yields

$$\mathrm{CRB}_{\theta\theta} = \frac{mc^2}{2\Omega_{\mathrm{c}}^2 \cdot \mathrm{SNR}} \cdot \begin{bmatrix} \dfrac{1}{Q\cos^2(\psi)} & 0 \\ 0 & \dfrac{1}{Q\sin^2(\psi) + Q_{zz}\cos^2(\psi)} \end{bmatrix} \tag{4.14a}$$

$$V_\zeta \sim \frac{1}{|x|^3} \cdot \frac{\tau^2}{Q\sqrt{\sin^2(\psi) + q_{zz}\cdot\cos^2(\psi)}} \tag{4.14b}$$

where $q_{zz} = Q_{zz}/Q$ is the moment-of-inertia parameter for the z axis, normalized by the moment-of-inertia parameter Q for the x and y axes.

We define the volume $v_\zeta = V_\zeta/(V_\zeta|_{\psi=\pi/2}) = (\sin^2\psi + q_{zz}\cdot\cos^2\psi)^{-1/2}$ of the confidence ellipsoid for the target's location $\boldsymbol{\zeta}$, normalized by the corresponding volume for a target lying along the z-axis ($\psi = \pi/2$). In addition, note that $V_\zeta|_{\psi=\pi/2}$ is independent of Q_{zz}, i.e., if the plane wave arrives along the z-axis, the volume of the confidence ellipsoid does not depend on the distribution of the sensors along this axis. In Fig. 4, we show plots of v_ζ as a function of $|\psi| \in [\pi/4, \pi/2]$ and $q_{zz} \in \{0, 0.5, 1, 2\}$ [note that $v_\zeta = v_\zeta(-\psi) = v_\zeta(\psi) = v_\zeta(|\psi|)$]. Performance independent of ψ is achieved for $q_{zz} = 1$. The case $q_{zz} = 0$ corresponds to a planar array lying in the x-y plane. The figure illustrates the performance improvements in terms of the volume of the confidence ellipsoid that can be achieved by using a 3-D array, compared with a planar array (of course, for $|\psi| = \pi/2$, there can be no improvement since, in that case, the confidence volume does not depend on q_{zz}).

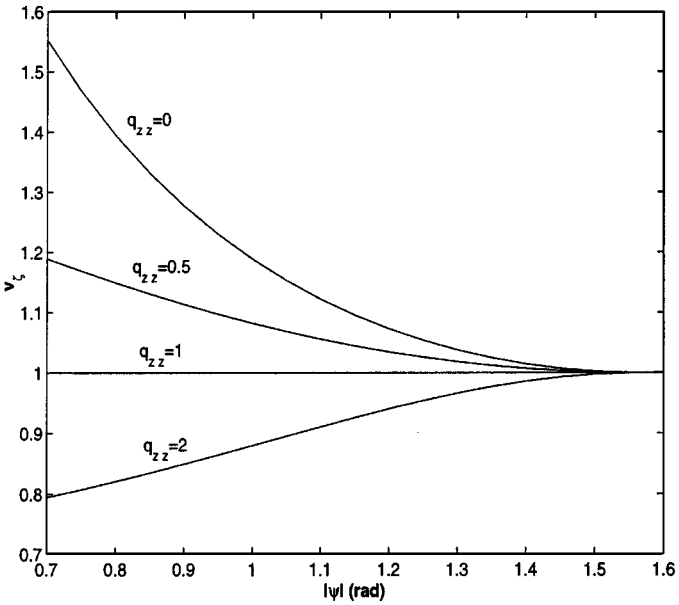

Fig. 4. Normalized volume v_ζ of the confidence ellipsoid for the target's location $\boldsymbol{\zeta}$ as a function of the elevation angle's magnitude $|\psi|$ and various values of normalized moment-of-inertia parameter for the z axis q_{zz}.

In Table I, we compare several 3-D arrays that satisfy the above azimuth-invariance conditions. The shapes of these arrays are shown in Fig. 5, and we assume that the sensors are uniformly distributed over a given volume. To avoid coupling, we do not allow the sensors to be closer than $\lambda/2$, where λ is the wavelength. This goal can be approximately achieved by allocating a cube with minimum volume $(\lambda/2)^3$ for each sensor. Then, the maximum number of sensors in the array is

$$m_{\mathrm{MAX}} = \frac{8V}{\lambda^3} \tag{4.15}$$

where V is the volume covered by the array; see also (4.6c). In the table, expressions for m_{MAX} are presented as a function of array geometry parameters for various configurations; see Appendix F for the derivation. Table I also shows Q and Q_{zz} as functions of the array geometry parameters.

To make a fair comparison between the different array configurations, we fix the number of sensors m and the maximum distance between the array elements, which is denoted by d_{MAX}. In Appendix F, we first derive the exact expressions for the volumes of the target location confidence ellipsoids. Then, to achieve the best possible performance of each array configuration (as well as for simplicity), we assume that the arrays are thin, i.e., the depth l and thickness w are much smaller than d_{MAX} (but larger than $\lambda/2$ to avoid coupling; see above). Under

TABLE I
MAXIMUM ARRAY SIZE m_{MAX}, MOMENT-OF-INERTIA PARAMETERS Q AND Q_{zz}, AND APPROXIMATE (FOR THIN ARRAYS) VOLUMES OF THE TARGET LOCATION CONFIDENCE ELLIPSOID (NORMALIZED WITH RESPECT TO THE SPHERICAL ARRAY) FOR THE ARRAY SHAPES IN FIG. 5

Array shape	m_{MAX}	Q	Q_{zz}	$\approx \frac{V_\zeta}{V_\zeta\vert_{\text{spherical array}}}$
Square plate	$\frac{4l(d_{\mathrm{MAX}}^2-l^2)}{\lambda^3}$	$\frac{m\cdot(d_{\mathrm{MAX}}^2-l^2)}{24}$	$\frac{ml^2}{12}$	$\frac{2}{\vert\sin\psi\vert}$
Circular plate	$\frac{2\pi l(d_{\mathrm{MAX}}^2-l^2)}{\lambda^3}$	$\frac{m\cdot(d_{\mathrm{MAX}}^2-l^2)}{16}$	$\frac{ml^2}{12}$	$\frac{4}{3\vert\sin\psi\vert}$
Spherical layer	$\frac{4\pi\left[d_{\mathrm{MAX}}^3-(d_{\mathrm{MAX}}-2w)^3\right]}{3\lambda^3}$	$\frac{m}{5}\cdot\frac{(d_{\mathrm{MAX}}/2)^5-(d_{\mathrm{MAX}}/2-w)^5}{(d_{\mathrm{MAX}}/2)^3-(d_{\mathrm{MAX}}/2-w)^3}$		1
Cylindrical ring	$\frac{8\pi\cdot l\cdot w\cdot\left(\sqrt{d_{\mathrm{MAX}}^2-l^2}-w\right)}{\lambda^3}$	$\frac{m\cdot u^2(d_{\mathrm{MAX}},w,l)}{16}$	$\frac{m}{12}\cdot l^2$	$\frac{2}{3\vert\sin\psi\vert}$
		$u^2(d_{\mathrm{MAX}},w,l)=d_{\mathrm{MAX}}^2-l^2+\left(\sqrt{d_{\mathrm{MAX}}^2-l^2}-2w\right)^2$		

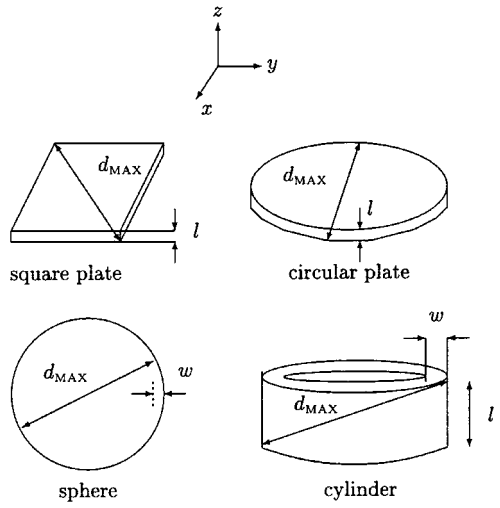

Fig. 5. Array geometries considered in Table I.

this assumption, we compute the approximate volume of the target location confidence ellipsoid, normalized with respect to the corresponding confidence volume for a spherical array ($V_\zeta/V_\zeta|_{\mathrm{sphere}}$); see Table I and Appendix F (where we compute the expressions for m_{MAX}, Q, and Q_{zz} as well). It follows that among the arrays in Fig. 5, only a thin cylindrical ring array can outperform the thin spherical array in the range of elevation angles $0.73 < |\psi| \leq \pi/2$ (i.e., elevations satisfying $2/3 < |\sin\psi| < 1$). Both cylindrical and spherical radar arrays have been built and analyzed [27], [29]–[32]. In addition, a spherical surface array was used for 3-D radio channel measurements [33], and a cylindrical array design was proposed for a mobile communications base station in [34].

As expected, the expressions for the above approximate normalized volumes become exact for $l = w = 0$; then, the square plate, circular plate, and spherical layer degenerate to corresponding surface arrays, whereas the cylindrical ring degenerates to a circular array. Note, however, that in this case, the maximum number of sensors m_{MAX} that can be placed on these arrays is significantly reduced, which influences the circular array in particular.

V. CONCLUDING REMARKS

We derived Cramér–Rao bound expressions for the range, velocity, and direction of a point target using an active radar or sonar array. First, general CRB expressions were derived for a narrowband signal and array model and a space-time separable noise model that allows both spatial and temporal correlation. Under these noise and signal models, we showed that the CRB for the direction parameters is independent of whether or not the time delay and Doppler shift are known, and vice versa. Then, we specialized the CRB results to the case of temporally white noise and a rectangular chirp pulse sequence. We also computed the CRB expressions for a 3-D array with identical isotropic sensors in spatially white noise. Under these conditions, we showed that these expressions are functions of the sensor placements only through "moment of inertia" parameters of the array. We proposed the volume of the confidence region for the target's location as a measure of accuracy and showed that if the noise is both spatially and temporally white, the highest accuracy is achieved for targets lying along one of the principal axes of inertia of the array. Finally, we compared the location accuracies of several 3-D array geometries.

Further research will include extending the CRB results to account for multiple targets (following [35]) or the wideband signal model (or both) and developing efficient estimation algorithms that exploit space-time factorability to reduce computational load.

APPENDIX A
CRB DERIVATION

To derive the CRB for $\boldsymbol{\theta}$ and $\boldsymbol{v}$, we start from a well-known expression for the Fisher information matrix in, for example [15,

p. 525], which, under the signal and noise model in Section II, simplifies to

$$\mathcal{I} = 2\,\mathrm{Re}\{D(\boldsymbol{\gamma})^*(C^{-1}\otimes\Sigma^{-1})D(\boldsymbol{\gamma})\} \quad \text{(A.1a)}$$

$$D(\boldsymbol{\gamma}) = \frac{\partial \boldsymbol{\mu}(\boldsymbol{\gamma})}{\partial \boldsymbol{\gamma}^T} = [D_x(\boldsymbol{\gamma}), D_{\boldsymbol{\theta}}(\boldsymbol{\gamma}), D_{\boldsymbol{v}}(\boldsymbol{\gamma})] \quad \text{(A.1b)}$$

$$D_x(\boldsymbol{\gamma}) = \left[\frac{\partial \boldsymbol{\mu}(\boldsymbol{\gamma})}{\partial\,\mathrm{Re}\{x\}}, \frac{\partial \boldsymbol{\mu}(\boldsymbol{\gamma})}{\partial\,\mathrm{Imag}\{x\}}\right] = [1, j]\otimes\boldsymbol{\phi}(\boldsymbol{v})\otimes\boldsymbol{a}(\boldsymbol{\theta}) \quad \text{(A.1c)}$$

$$D_{\boldsymbol{\theta}}(\boldsymbol{\gamma}) = \frac{\partial \boldsymbol{\mu}(\boldsymbol{\gamma})}{\partial \boldsymbol{\theta}^T} = x\cdot\boldsymbol{\phi}(\boldsymbol{\gamma})\otimes\frac{\partial \boldsymbol{a}(\boldsymbol{\theta})}{\partial \boldsymbol{\theta}^T} \quad \text{(A.1d)}$$

$$D_{\boldsymbol{v}}(\boldsymbol{\gamma}) = \frac{\partial \boldsymbol{\mu}(\boldsymbol{\gamma})}{\partial \boldsymbol{v}^T} = x\cdot\frac{\partial \boldsymbol{\phi}(\boldsymbol{v})}{\partial \boldsymbol{v}^T}\otimes\boldsymbol{a}(\boldsymbol{\theta}) \quad \text{(A.1e)}$$

where $\mathcal{I}$ is the FIM for target parameters $\boldsymbol{\gamma}$. The above FIM can be written as

$$\mathcal{I} = \begin{bmatrix} \mathcal{I}_{xx} & \mathcal{I}_{\boldsymbol{\theta}x}^{\mathrm{T}} & \mathcal{I}_{\boldsymbol{v}x}^{\mathrm{T}} \\ \mathcal{I}_{\boldsymbol{\theta}x} & \mathcal{I}_{\theta\theta} & \mathcal{I}_{\boldsymbol{v}\theta}^{\mathrm{T}} \\ \mathcal{I}_{\boldsymbol{v}x} & \mathcal{I}_{\boldsymbol{v}\theta} & \mathcal{I}_{\boldsymbol{v}\boldsymbol{v}} \end{bmatrix} \quad \text{(A.2)}$$

where

$$\mathcal{I}_{xx} = 2\cdot\boldsymbol{\phi}(\boldsymbol{v})^*C^{-1}\boldsymbol{\phi}(\boldsymbol{v})\cdot\boldsymbol{a}(\boldsymbol{\theta})^*\Sigma^{-1}\boldsymbol{a}(\boldsymbol{\theta})\cdot I_2 \quad \text{(A.3a)}$$

$$\mathcal{I}_{\boldsymbol{\theta}x} = \mathrm{Re}\{[1, j]\otimes P_{\boldsymbol{\theta}x}\} \quad \text{(A.3b)}$$

$$\mathcal{I}_{\theta\theta} = 2|x|^2\cdot\boldsymbol{\phi}(\boldsymbol{v})^*C^{-1}\boldsymbol{\phi}(\boldsymbol{v}) \cdot\mathrm{Re}\left\{\frac{\partial \boldsymbol{a}(\boldsymbol{\theta})^*}{\partial \boldsymbol{\theta}}\Sigma^{-1}\frac{\partial \boldsymbol{a}(\boldsymbol{\theta})}{\partial \boldsymbol{\theta}^T}\right\} \quad \text{(A.3c)}$$

$$\mathcal{I}_{\boldsymbol{v}x} = \mathrm{Re}\{[1, j]\otimes P_{\boldsymbol{v}x}\} \quad \text{(A.3d)}$$

$$\mathcal{I}_{\boldsymbol{v}\theta} = \mathrm{Re}\{P_{\boldsymbol{v}\theta}\} \quad \text{(A.3e)}$$

$$\mathcal{I}_{\boldsymbol{v}\boldsymbol{v}} = \mathrm{Re}\{P_{\boldsymbol{v}\boldsymbol{v}}\} \quad \text{(A.3f)}$$

and

$$P_{\boldsymbol{\theta}x} = 2\cdot\boldsymbol{\phi}(\boldsymbol{v})^*C^{-1}\boldsymbol{\phi}(\boldsymbol{v})\cdot x^*\cdot\frac{\partial \boldsymbol{a}(\boldsymbol{\theta})^*}{\partial \boldsymbol{\theta}}\Sigma^{-1}\boldsymbol{a}(\boldsymbol{\theta} \quad \text{(A.4a)}$$

$$P_{\boldsymbol{v}x} = 2x^*\cdot\boldsymbol{a}(\boldsymbol{\theta})^*\Sigma^{-1}\boldsymbol{a}(\boldsymbol{\theta})\cdot\frac{\partial \boldsymbol{\phi}(\boldsymbol{v})^*}{\partial \boldsymbol{v}}C^{-1}\boldsymbol{\phi}(\boldsymbol{v}) \quad \text{(A.4b)}$$

$$P_{\boldsymbol{v}\theta} = 2|x|^2\cdot\frac{\partial \boldsymbol{\phi}(\boldsymbol{v})^*}{\partial \boldsymbol{v}}C^{-1}\boldsymbol{\phi}(\boldsymbol{v})\cdot\boldsymbol{a}(\boldsymbol{\theta})^*\Sigma^{-1}\frac{\partial \boldsymbol{a}(\boldsymbol{\theta})}{\partial \boldsymbol{\theta}^T} \quad \text{(A.4c)}$$

$$P_{\boldsymbol{v}\boldsymbol{v}} = 2|x|^2\cdot\boldsymbol{a}(\boldsymbol{\theta})^*\Sigma^{-1}\boldsymbol{a}(\boldsymbol{\theta})\cdot\frac{\partial \boldsymbol{\phi}(\boldsymbol{v})^*}{\partial \boldsymbol{v}}C^{-1}\frac{\partial \boldsymbol{\phi}(\boldsymbol{v})}{\partial \boldsymbol{v}^T}. \quad \text{(A.4d)}$$

Now, since the signal and additive noise parameters are disjoint, the CRB for signal vector $\boldsymbol{\gamma}$ is computed simply as $\mathrm{CRB} = \mathcal{I}^{-1}$. We will use the same block partitioning of the CRB as for $\mathcal{I}$ in (A.2).

We now compute the CRB for the DOA, Doppler shift, and time delay

$$\mathrm{CRB}_{\boldsymbol{\theta}\boldsymbol{v},\boldsymbol{\theta}\boldsymbol{v}} = \begin{bmatrix} \mathrm{CRB}_{\theta\theta} & \mathrm{CRB}_{\boldsymbol{v}\theta}^{\mathrm{T}} \\ \mathrm{CRB}_{\boldsymbol{v}\theta} & \mathrm{CRB}_{\boldsymbol{v}\boldsymbol{v}} \end{bmatrix} = \left\{\begin{bmatrix} \mathcal{I}_{\theta\theta} & \mathcal{I}_{\boldsymbol{v}\theta}^{\mathrm{T}} \\ \mathcal{I}_{\boldsymbol{v}\theta} & \mathcal{I}_{\boldsymbol{v}\boldsymbol{v}} \end{bmatrix} - \mathcal{J}\mathcal{I}_{xx}^{-1}\mathcal{J}^T\right\}^{-1} \quad \text{(A.5)}$$

where $\mathcal{J} = [\mathcal{I}_{\boldsymbol{\theta}x}^{\mathrm{T}}, \mathcal{I}_{\boldsymbol{v}x}^{\mathrm{T}}]^T$. Using

$$\mathcal{J}\mathcal{I}_{xx}^{-1}\mathcal{J}^T = \frac{1}{2\cdot\boldsymbol{\phi}(\boldsymbol{v})^*C^{-1}\boldsymbol{\phi}(\boldsymbol{v})\cdot\boldsymbol{a}(\boldsymbol{\theta})^*\Sigma^{-1}\boldsymbol{a}(\boldsymbol{\theta})} \cdot\begin{bmatrix} \mathrm{Re}\{P_{\boldsymbol{\theta}x}P_{\boldsymbol{\theta}x}^*\} & \mathrm{Re}\{P_{\boldsymbol{\theta}x}P_{\boldsymbol{v}x}^*\} \\ \mathrm{Re}\{P_{\boldsymbol{v}x}P_{\boldsymbol{\theta}x}^*\} & \mathrm{Re}\{P_{\boldsymbol{v}x}P_{\boldsymbol{v}x}^*\} \end{bmatrix} \quad \text{(A.6)}$$

it easily follows that

$$\mathcal{I}_{\boldsymbol{v}\theta} - \frac{1}{2\cdot\boldsymbol{\phi}(\boldsymbol{v})^*C^{-1}\boldsymbol{\phi}(\boldsymbol{v})\cdot\boldsymbol{a}(\boldsymbol{\theta})^*\Sigma^{-1}\boldsymbol{a}(\boldsymbol{\theta})} \cdot\mathrm{Re}\{P_{\boldsymbol{v}x}P_{\boldsymbol{\theta}x}^*\} = 0 \quad \text{(A.7)}$$

i.e., $\mathrm{CRB}_{\boldsymbol{v}\theta} = 0$; see also (3.1b). Thus $\mathrm{CRB}_{\boldsymbol{\theta}\boldsymbol{v},\boldsymbol{\theta}\boldsymbol{v}}$ is block-diagonal, implying that

$$\mathrm{CRB}_{\theta\theta} = \left[\mathcal{I}_{\theta\theta} - \frac{1}{2\cdot\boldsymbol{\phi}(\boldsymbol{v})^*C^{-1}\boldsymbol{\phi}(\boldsymbol{v})\cdot\boldsymbol{a}(\boldsymbol{\theta})^*\Sigma^{-1}\boldsymbol{a}(\boldsymbol{\theta})} \cdot\mathrm{Re}\{P_{\boldsymbol{\theta}x}P_{\boldsymbol{\theta}x}^*\}\right]^{-1} \quad \text{(A.8a)}$$

$$\mathrm{CRB}_{\boldsymbol{v}\upsilon} = \left[\mathcal{I}_{\boldsymbol{v}\boldsymbol{v}} - \frac{1}{2\cdot\boldsymbol{\phi}(\boldsymbol{v})^*C^{-1}\boldsymbol{\phi}(\boldsymbol{v})\cdot\boldsymbol{a}(\boldsymbol{\theta})^*\Sigma^{-1}\boldsymbol{a}(\boldsymbol{\theta})} \cdot\mathrm{Re}\{P_{\boldsymbol{v}x}P_{\boldsymbol{v}x}^*\}\right]^{-1} \quad \text{(A.8b)}$$

and the expressions in (3.1a) and (3.1c) follow directly.

A. CRB on the Target's Radial Velocity for a Moving Array

We derive the CRB for the Doppler shift due to the radial component of target's velocity (denoted by ω_{DT}) for the case when the array moves with constant velocity; see Section III-A1.

Using (3.1) and $\omega_{\mathrm{DT}} = \omega_{\mathrm{D}} + \omega_{\mathrm{D}A}\cos[\varphi(\boldsymbol{\theta})]$ from Section III-A1, we compute

$$\mathrm{CRB}_{\omega_{\mathrm{DT}}\omega_{\mathrm{DT}}} = \begin{bmatrix} \frac{\partial \omega_{\mathrm{DT}}}{\partial \boldsymbol{\theta}^T} & \frac{\partial \omega_{\mathrm{DT}}}{\partial \omega_{\mathrm{D}}} \end{bmatrix}\cdot\begin{bmatrix} \mathrm{CRB}_{\theta\theta} & 0 \\ 0 & \mathrm{CRB}_{\omega_{\mathrm{D}}\omega_{\mathrm{D}}} \end{bmatrix} \cdot\begin{bmatrix} \frac{\partial \omega_{\mathrm{DT}}}{\partial \boldsymbol{\theta}} \\ \frac{\partial \omega_{\mathrm{DT}}}{\partial \omega_{\mathrm{D}}} \end{bmatrix} \quad \text{(A.9)}$$

and (3.4) easily follows by using $\partial\omega_{\mathrm{DT}}/\partial\boldsymbol{\theta}^T = \omega_{\mathrm{D}A}\sin[\varphi(\boldsymbol{\theta})]\cdot d\varphi(\boldsymbol{\theta})/d\boldsymbol{\theta}^T$ and $\partial\omega_{\mathrm{DT}}/\partial\omega_{\mathrm{D}} = 1$.

B. CRB for Temporally White Noise

We specialize the general CRB expression (3.1c) to temporally white noise (i.e., $C = I_N$) and signal model in (2.1). Let $d[n] = ds[n]/dn = \Delta t\cdot ds(t)/dt|_{t=n\Delta t}$, and define

$$\varepsilon = \Delta t\cdot\sum_{n=1}^{N}|s[n-n_\tau]|^2 \quad \text{(A.10a)}$$

$$\delta = (\Delta t)^3\cdot\sum_{n=1}^{N}n^2\cdot|s[n-n_\tau]|^2 - \frac{1}{\varepsilon}\cdot\left[(\Delta t)^2\cdot\sum_{n=1}^{N}n\cdot|s[n-n_\tau]|^2\right]^2 \quad \text{(A.10b)}$$

$$\xi = \Delta t \cdot \sum_{n=1}^{N} n \cdot s[n-n_\tau] d[n-n_\tau]^* - (\Delta t)^2 \cdot \frac{1}{\varepsilon} \cdot \sum_{n=1}^{N} n |s[n-n_\tau]|^2 \cdot \sum_{n=1}^{N} s[n-n_\tau] d[n-n_\tau]^* \tag{A.10c}$$

$$\beta = \frac{1}{\Delta t} \cdot \sum_{n=1}^{N} |d[n-n_\tau]|^2 - \frac{1}{\varepsilon} \cdot \left| \sum_{n=1}^{N} s[n-n_\tau] d[n-n_\tau]^* \right|^2. \tag{A.10d}$$

Then, the expressions in (3.1a) and (3.1c) simplify to (see also [10])

$$\begin{aligned} \mathrm{CRB}_{\theta\theta} &= \frac{1}{2|x|^2 \sum_{n=1}^{N} |s[n-n_\tau]|^2} \left[\mathrm{Re} \left\{ \frac{\partial \boldsymbol{a}(\boldsymbol{\theta})^*}{\partial \boldsymbol{\theta}} \cdot \Sigma^{-1/2} \Pi_a^{\perp}(\boldsymbol{\theta}, \Sigma) \Sigma^{-1/2} \frac{\partial \boldsymbol{a}(\boldsymbol{\theta})}{\partial \boldsymbol{\theta}^T} \right\} \right]^{-1} \\ &= \frac{\boldsymbol{a}(\boldsymbol{\theta})^* \Sigma^{-1} \boldsymbol{a}(\boldsymbol{\theta})}{2 \cdot \mathrm{SNR}} \left[\mathrm{Re} \left\{ \frac{\partial \boldsymbol{a}(\boldsymbol{\theta})^*}{\partial \boldsymbol{\theta}} \cdot \Sigma^{-1/2} \Pi_a^{\perp}(\boldsymbol{\theta}, \Sigma) \Sigma^{-1/2} \frac{\partial \boldsymbol{a}(\boldsymbol{\theta})}{\partial \boldsymbol{\theta}^T} \right\} \right]^{-1} \end{aligned} \tag{A.11a}$$

$$\begin{aligned} \mathrm{CRB}_{\boldsymbol{vv}} &= \frac{1}{2|x|^2 \cdot \boldsymbol{a}(\boldsymbol{\theta})^* \Sigma^{-1} \boldsymbol{a}(\boldsymbol{\theta})} \cdot \begin{bmatrix} (1/\Delta t)^3 \cdot \delta & (1/\Delta t) \cdot \mathrm{Imag}\{\xi\} \\ (1/\Delta t) \cdot \mathrm{Imag}\{\xi\} & \Delta t \cdot \beta \end{bmatrix}^{-1} \\ &= \frac{\varepsilon}{2 \cdot \mathrm{SNR}} \begin{bmatrix} (1/\Delta t)^2 \cdot \delta & \mathrm{Imag}\{\xi\} \\ \mathrm{Imag}\{\xi\} & (\Delta t)^2 \cdot \beta \end{bmatrix}^{-1} \end{aligned} \tag{A.11b}$$

and the SNR in (3.5) simplifies to

$$\mathrm{SNR} = |x|^2 \cdot \sum_{n=1}^{N} |s[n-n_\tau]|^2 \cdot \boldsymbol{a}(\boldsymbol{\theta})^* \Sigma^{-1} \boldsymbol{a}(\boldsymbol{\theta}). \tag{A.12}$$

Appendix B
Ambiguity Function Derivation

We derive the ambiguity function for the signal and noise models in Section II. First, we introduce the following measure of separation between the probability density functions of the measurements corresponding to two targets with parameters $\boldsymbol{\gamma}_0 = [\mathrm{Re}\{x_0\}, \mathrm{Imag}\{x_0\}, \boldsymbol{\theta}_0^T, \boldsymbol{v}_0^T]^T$ and $\boldsymbol{\gamma} = [\mathrm{Re}\{x\}, \mathrm{Imag}\{x\}, \boldsymbol{\theta}^T, \boldsymbol{v}^T]^T$ (assuming fixed noise covariance $C \otimes \Sigma$)

$$d(\boldsymbol{\gamma}, \boldsymbol{\gamma}_0) = [\boldsymbol{\mu}(\boldsymbol{\gamma}) - \boldsymbol{\mu}(\boldsymbol{\gamma}_0)]^* (C^{-1} \otimes \Sigma^{-1}) [\boldsymbol{\mu}(\boldsymbol{\gamma}) - \boldsymbol{\mu}(\boldsymbol{\gamma}_0)]. \tag{B.1}$$

This measure is by definition the square of the Mahalanobis distance; it is also the Kullback-directed divergence, which is used in [16]. Additionally, the identifiability by distribution (see [36]) of the target parameters $\boldsymbol{\gamma}$ reduces to the following requirement: $d(\boldsymbol{\gamma}, \boldsymbol{\gamma}_0) = 0$ if and only if $\boldsymbol{\gamma} = \boldsymbol{\gamma}_0$. Minimizing the distance in (B.1) with respect to the nuisance parameter x yields

$$\begin{aligned} \hat{d}_{x_0}([\boldsymbol{\theta}^T, \boldsymbol{v}^T]^T, [\boldsymbol{\theta}_0^T, \boldsymbol{v}_0^T]^T) &= |x_0|^2 \cdot \boldsymbol{\phi}(\boldsymbol{v}_0)^* C^{-1} \boldsymbol{\phi}(\boldsymbol{v}_0) \cdot \boldsymbol{a}(\boldsymbol{\theta}_0)^* \Sigma^{-1} \boldsymbol{a}(\boldsymbol{\theta}_0) \\ &\quad - |x_0|^2 \cdot \frac{|\boldsymbol{\phi}(\boldsymbol{v}_0)^* C^{-1} \boldsymbol{\phi}(\boldsymbol{v})|^2 \cdot |\boldsymbol{a}(\boldsymbol{\theta}_0)^* \Sigma^{-1} \boldsymbol{a}(\boldsymbol{\theta})|^2}{\boldsymbol{\phi}(\boldsymbol{v})^* C^{-1} \boldsymbol{\phi}(\boldsymbol{v}) \cdot \boldsymbol{a}(\boldsymbol{\theta})^* \Sigma^{-1} \boldsymbol{a}(\boldsymbol{\theta})}. \end{aligned} \tag{B.2}$$

Now, according to [16, Def. 2], the generalized ambiguity function is computed as

$$\mathcal{A}([\boldsymbol{\theta}^T, \boldsymbol{v}^T]^T, [\boldsymbol{\theta}_0^T, \boldsymbol{v}_0^T]^T) = 1 - \frac{\hat{d}_{x_0}([\boldsymbol{\theta}^T, \boldsymbol{v}^T]^T, [\boldsymbol{\theta}_0^T, \boldsymbol{v}_0^T]^T)}{[\hat{d}_{x_0}([\boldsymbol{\theta}_0^T, \boldsymbol{v}_0^T]^T)]_{\mathrm{ub}}} \tag{B.3}$$

where $[\hat{d}_{x_0}([\boldsymbol{\theta}_0^T, \boldsymbol{\eta}_0^T]^T)]_{\mathrm{ub}}$ is the upper bound on the distance in (B.2). Since the signal is of finite duration, for sufficiently large time delay difference $\tau - \tau_0$, we have

$$\hat{d}_{x_0}([\boldsymbol{\theta}_0^T, \boldsymbol{v}_0^T]^T)]_{\mathrm{ub}} = |x_0|^2 \cdot \boldsymbol{\phi}(\boldsymbol{v}_0)^* C^{-1} \boldsymbol{\phi}(\boldsymbol{v}_0) \cdot \boldsymbol{a}(\boldsymbol{\theta}_0)^* \Sigma^{-1} \boldsymbol{a}(\boldsymbol{\theta}_0). \tag{B.4}$$

The ambiguity function in (3.6) follows by substituting (B.2) and (B.4) into (B.3).

Appendix C
CRB Derivation for a Chirp Sequence

We derive the CRB for time delay and Doppler shift for a sequence of chirp pulses in temporally white noise, as shown in (3.16). Using the signal shape in (3.14), (3.11a), and (3.11b), we obtain

$$\varepsilon = \int_{-\infty}^{\infty} |s(t)|^2 \, dt = PT_0 \tag{C.1a}$$

$$\begin{aligned} \delta &= \sum_{p=0}^{P-1} \int_{pT_\mathrm{R}}^{pT_\mathrm{R}+T_0} t^2 \, dt - \frac{1}{PT_0} \left| \sum_{p=0}^{P-1} \int_{pT_\mathrm{R}}^{pT_\mathrm{R}+T_0} t \, dt \right|^2 \\ &= \frac{T_0^3 P}{12} \cdot \left[1 + \left(\frac{T_\mathrm{R}}{T_0} \right)^2 (P^2 - 1) \right]. \end{aligned} \tag{C.1b}$$

Note that using the time translation invariance property of expressions (3.11), we computed ε and δ in (C.1), assuming $\tau = 0$. From $\int_{-\infty}^{\infty} s(t-\tau) \cdot ds(t-\tau)^*/dt \cdot dt = 0$ and (3.11c) and (3.11d), it follows that

$$-\mathrm{Imag}\{\xi\} = -\mathrm{Imag} \left\{ \int_{-\infty}^{\infty} t s(t) \frac{ds(t)^*}{dt} dt \right\} = P \cdot \frac{\pi f_\mathrm{B} T_0^2}{6} \tag{C.2a}$$

$$\beta = P \cdot \int_{-\infty}^{\infty} \Omega^2 |S_0(\Omega)|^2 \, df \approx P \cdot \frac{\pi^2 f_\mathrm{B}^2 T_0}{3}. \tag{C.2b}$$

The third expression in (C.2b) holds when the time-bandwidth product of a pulse is large, i.e., $T_0 f_\mathrm{B} \gg 1$. Then, the spectrum of a pulse approaches a rectangular distribution [2, p. 139 and p. 302], which can be approximated as $|S_0(\Omega)|^2 = T_0/f_\mathrm{B} \cdot [h(f + f_\mathrm{B}/2) - h(f - f_\mathrm{B}/2)]$ (see, e.g., [21, eq. (39)]), yielding the

approximate expression in (C.2b). Based on (C.1), (C.2), and (3.10b), $\mathrm{CRB}_{\boldsymbol{\eta\eta}}$ in (3.16) easily follows.

Appendix D
Wald Tests and Volume of the Linearized Confidence Region

We show how to construct a linearized confidence region for the target location and compute its volume using Wald tests. The linearized confidence region (in the form of an elliposoid) for testing H_0: $\boldsymbol{h}(\boldsymbol{\gamma}) = \mathbf{0}$, where $\boldsymbol{h}$ is a once continuously-differentiable function, is defined as

$$T^2(\boldsymbol{\gamma}) = \boldsymbol{h}(\boldsymbol{\gamma})^T [H(\boldsymbol{\gamma}) \cdot \mathrm{CRB} \cdot H(\boldsymbol{\gamma})^T]^{-1} \boldsymbol{h}(\boldsymbol{\gamma}) \leq g \quad \text{(D.1)}$$

where $H(\boldsymbol{\gamma}) = \partial \boldsymbol{h}(\boldsymbol{\gamma})/\partial \boldsymbol{\gamma}^T$, $\mathrm{CRB} = \mathcal{I}^{-1}$ [see also (A.2) and (A.3) in Appendix A], and g is the threshold computed to satisfy a desired probability of false alarm [37], [38, ch. 6e.3], [39, ch. 7.3.3]. From (D.1), testing H_0: $\boldsymbol{\gamma} = \boldsymbol{\gamma}_0$ yields the confidence ellipsoid of the following form: $(\boldsymbol{\gamma} - \boldsymbol{\gamma}_0)^T \mathrm{CRB}^{-1} (\boldsymbol{\gamma} - \boldsymbol{\gamma}_0) \leq g$. Obviously, the squared volume of this ellipsoid is proportional to $|\mathrm{CRB}|$. Similarly, from (D.1), it follows that testing H_0: $\boldsymbol{\zeta}(\boldsymbol{\alpha}) - \boldsymbol{\zeta}(\boldsymbol{\alpha}_0) = 0$ yields the confidence ellipsoid with squared volume proportional to $|\mathrm{CRB}_{\boldsymbol{\zeta\zeta}}| = |\partial \boldsymbol{\zeta}/\partial \boldsymbol{\alpha}^T \cdot \mathrm{CRB}_{\boldsymbol{\alpha\alpha}} \cdot \partial \boldsymbol{\zeta}^T/\partial \boldsymbol{\alpha}|$, and (4.9) follows.

Appendix E
Volume of the Confidence Ellipsoid for the Target's Location in Cartesian Coordinates

We compute the volume of the confidence ellipsoid for the target's location as a function of the target's coordinates in a Cartesian coordinate system, whose axes are chosen to be the principal axes of inertia of the array.

The array geometry parameters Q_{xx}, Q_{xy}, Q_{xz}, Q_{yy}, Q_{yz}, and Q_{zz} define the moment of inertia tensor of the array where each sensor is assigned a unit mass; see [26, ch. 6]. The tensor of inertia can be reduced to diagonal form by an appropriate choice of axes x, y, and z; these directions are called the *principal axes of inertia* [26, ch. 6]. In this case, $Q_{xy} = Q_{xz} = Q_{yz} = 0$, which significantly simplifies the expressions in (4.5)

$$W_{11} = \frac{\cos^2\psi}{c^2}(Q_{xx}\sin^2\phi + Q_{yy}\cos^2\phi) \quad \text{(E.1a)}$$

$$W_{12} = \frac{\cos\psi}{2c^2} \cdot (Q_{xx} - Q_{yy}) \sin 2\phi \sin\psi \quad \text{(E.1b)}$$

$$W_{22} = \frac{1}{c^2} \cdot [(Q_{xx}\cos^2\phi + Q_{yy}\sin^2\phi)\sin^2\psi + Q_{zz}\cos^2\psi] \quad \text{(E.1c)}$$

yielding

$$\begin{aligned} &\frac{c^6\tau^2}{4} \cdot \frac{W_{11}W_{22} - W_{12}^2}{\cos^2\psi} \\ &\quad = \left(\frac{c\tau}{2}\right)^2 \cdot [Q_{zz}(Q_{xx}\sin^2\phi + Q_{yy}\cos^2\phi) \\ &\qquad \cdot \cos^2\psi + Q_{xx}Q_{yy} \cdot \sin^2\psi] \\ &\quad = Q_{zz}Q_{xx} \cdot y_{\mathrm{T}}^2 + Q_{yy}Q_{zz} \cdot x_{\mathrm{T}}^2 + Q_{xx}Q_{yy} \cdot z_{\mathrm{T}}^2. \end{aligned} \quad \text{(E.2a)}$$

Using the above equality, (4.7), and (4.11), we get (4.12). Now, it is obvious that for a fixed range (i.e., $\rho = c\tau/2 = \sqrt{x_{\mathrm{T}}^2 + y_{\mathrm{T}}^2 + z_{\mathrm{T}}^2} = \text{const}$), the volume V_ζ of the confidence ellipsoid for the target location in (4.12) is minimized for a target lying on one of the principal axes. This axis (which defines the most desirable DOA) is the one for which the product of the moment-of-inertia parameters for the other two axes is maximized, i.e., it is the x-axis if $Q_{yy}Q_{zz} = \max\{Q_{xx}Q_{yy}, Q_{yy}Q_{zz}, Q_{zz}Q_{xx}\}$ and likewise for the other two cases.

Analogously, the least desirable DOA (i.e., the one with maximum volume of the confidence ellipsoid) is along the principal axis for which the product of the moment-of-inertia parameters for the other two axes is minimized. In addition, note that the most and the least desirable DOA are always orthogonal since they lie along two principal axes.

Appendix F
$\mathrm{CRB}_{\theta\theta}$ Derivation for Several Array Configurations

We derive the CRB expressions and confidence volumes for the target location for several 3-D arrays of identical isotropic sensors (whose shapes are shown in Fig. 5) in spatially white noise.

We first derive the properties of an array in the form of a spherical layer and then use the performance of this array as a reference for comparison with other array configurations. The comparison is performed assuming the same number of sensors m and maximum distance d_{MAX} between the array elements for all arrays.

For a spherical layer array with radius R and thickness w, we have $d_{\mathrm{MAX}} = 2R$ and $V = 4\pi/3 \cdot [R^3 - (R-w)^3] = 4\pi/3 \cdot [d_{\mathrm{MAX}}^3/8 - (d_{\mathrm{MAX}}/2 - w)^3]$, yielding

$$\begin{aligned} m_{\mathrm{MAX}} &= \frac{4\pi[d_{\mathrm{MAX}}^3 - (d_{\mathrm{MAX}} - 2w)^3]}{3\lambda^3} \\ &\approx \frac{8\pi d_{\mathrm{MAX}}^2 w}{\lambda^3} \end{aligned} \quad \text{(F.1a)}$$

$$\begin{aligned} Q &= Q_{xx} = Q_{yy} = Q_{zz} \\ &= \frac{m}{V} \cdot \pi \cdot \int_{R-w}^{R} r^4\,dr \cdot \int_{-\pi/2}^{\pi/2} \cos^3\psi\,d\psi \\ &= \frac{m}{3} \cdot \frac{\frac{1}{5}[R^5 - (R-w)^5]}{\frac{1}{3}[R^3 - (R-w)^3]} \\ &= \frac{m}{5} \cdot \frac{(d_{\mathrm{MAX}}/2)^5 - (d_{\mathrm{MAX}}/2 - w)^5}{(d_{\mathrm{MAX}}/2)^3 - (d_{\mathrm{MAX}}/2 - w)^3} \\ &\approx \frac{m d_{\mathrm{MAX}}^2}{12}. \end{aligned} \quad \text{(F.1b)}$$

See (4.6) and (4.15). The approximate formulas above hold for a thin spherical layer, i.e., for $w \ll d_{\mathrm{MAX}}$.

Next, consider two plate arrays with depth l: a square and a circular plate. For a square plate array with x and y coordinates ranging from $-R$ to R and z ranging from $-l/2$ to $l/2$, we have $d_{\mathrm{MAX}} = \sqrt{8R^2 + l^2} \approx 2\sqrt{2} \cdot R$ and $V = 4R^2 l$, yielding

$$m_{\mathrm{MAX}} = \frac{4l(d_{\mathrm{MAX}}^2 - l^2)}{\lambda^3} \approx \frac{4l d_{\mathrm{MAX}}^2}{\lambda^3} \quad \text{(F.2a)}$$

$$Q = Q_{xx} = \frac{m}{V} \cdot \int_{-R}^{R} x^2\,dx \cdot 2Rl = \frac{mR^2}{3} = \frac{m \cdot (d_{\mathrm{MAX}}^2 - l^2)}{24} \approx \frac{m \cdot d_{\mathrm{MAX}}^2}{24} \tag{F.2b}$$

$$Q_{zz} = \frac{ml^2}{12} \tag{F.2c}$$

$$\frac{V_\zeta}{V_\zeta|_{\mathrm{spherical\,array}}} \approx \frac{2}{|\sin\psi|} > 1 \tag{F.2d}$$

where approximate expressions hold for a thin plate, i.e., $l \ll d_{\mathrm{MAX}}$. From the last equation above, it follows that for fixed maximum distance d_{MAX} between the sensors and array size m, the thin square array is significantly outperformed by the thin spherical array. Similarly, for a circular plate array of radius R (and z ranging from $-l/2$ to $l/2$), we have $d_{\mathrm{MAX}} = \sqrt{4R^2 + l^2} \approx 2R$ and $V = \pi l R^2$, yielding

$$m_{\mathrm{MAX}} = \frac{2\pi l(d_{\mathrm{MAX}}^2 - l^2)}{\lambda^3} \approx \frac{2\pi l d_{\mathrm{MAX}}^2}{\lambda^3} \tag{F.3a}$$

$$Q = \frac{m}{V} \cdot \frac{1}{2} l \cdot \int_{r=0}^{R} r^2 2\pi r\,dr = \frac{mR^2}{4} = \frac{m \cdot (d_{\mathrm{MAX}}^2 - l^2)}{16} \approx \frac{m \cdot d_{\mathrm{MAX}}^2}{16} \tag{F.3b}$$

$$Q_{zz} = \frac{ml^2}{12} \tag{F.3c}$$

$$\frac{V_\zeta}{V_\zeta|_{\mathrm{spherical\,array}}} \approx \frac{4}{3|\sin\psi|} > 1. \tag{F.3d}$$

Again, the circular plate array is significantly outperformed by the spherical layer array.

To outperform the spherical layer array in a particular range of directions, we can use an array of sensors distributed on a cylindrical ring with radius R, thickness w, and depth l along the most likely direction to the target. Let the most likely direction to the target be from elevation $\psi = \pi/2$ (i.e., along the z axis; see Fig. 5), and thus choose the cylinder lying along the z axis. Therefore, we have $d_{\mathrm{MAX}} = \sqrt{4R^2 + l^2} \approx 2R$ and $V = \pi l[R^2 - (R-w)^2] = \pi l w(2R - w) \approx 2\pi l w R$, and

$$m_{\mathrm{MAX}} = \frac{8\pi l \cdot w \cdot \left(\sqrt{d_{\mathrm{MAX}}^2 - l^2} - w\right)}{\lambda^3} \approx \frac{8\pi l \cdot w \cdot d_{\mathrm{MAX}}}{\lambda^3} \tag{F.4a}$$

$$Q = Q_{xx} = Q_{yy} = \frac{m}{V} \cdot l \cdot \pi \cdot \int_{R-w}^{R} r^3\,dr = \frac{m \cdot [R^2 + (R-w)^2]}{4} = \frac{m \cdot u^2(d_{\mathrm{MAX}}, w, l)}{16} \tag{F.4b}$$

$$u^2(d_{\mathrm{MAX}}, w, l) = d_{\mathrm{MAX}}^2 - l^2 + \left(\sqrt{d_{\mathrm{MAX}}^2 - l^2} - 2w\right)^2 \approx 2d_{\mathrm{MAX}}^2 \tag{F.4c}$$

$$Q_{zz} = \frac{ml^2}{12} \tag{F.4d}$$

$$\frac{V_\zeta}{V_\zeta|_{\mathrm{spherical\,array}}} \approx \frac{2}{3|\sin\psi|} \tag{F.4e}$$

where the approximate formulas hold for a thin ring, i.e., when $l \ll d_{\mathrm{MAX}}$ and $w \ll d_{\mathrm{MAX}}$.

Obviously, we need $u^2(d_{\mathrm{MAX}}, w, l) > \frac{4}{3} d_{\mathrm{MAX}}^2$ to outperform the spherical array at elevation $\psi = \pi/2$ with the same maximum distance between the sensors and array size m. Note that $u^2(d_{\mathrm{MAX}}, w, l)$ is a decreasing function of both l and w. However, these dimensions are necessary to allow a large number of antennas in the array, see (F.4a); otherwise, for $l = w = 0$, this array degenerates to a circular array (which cannot accomodate many sensors).

The results derived in this appendix are summarized in Table I.

ACKNOWLEDGMENT

We are grateful to the anonymous reviewers for their helpful comments.

REFERENCES

[1] H. L. Van Trees, *Detection, Estimation and Modulation Theory*. New York: Wiley, 1971, pt. III.

[2] C. E. Cook and M. Bernfeld, *Radar Signals: An Introduction to Theory and Application*. Boston, MA: Artech House, 1993.

[3] E. J. Kelly, "The radar measurement of range, velocity and acceleration," *IRE Trans. Military Electron.*, vol. ME-5, pp. 51–57, 1961.

[4] S. Haykin and A. Steinhardt, *Adaptive Radar Detection and Estimation*. New York: Wiley, 1992.

[5] S. Haykin, J. Litva, and T. Shepherd, *Radar Array Processing*. New York: Springer-Verlag, 1993.

[6] J. Ward, "Space-time adaptive processing for airborne radar," Lincoln Lab., Mass. Inst. Technol., Lexington, Tech. Rep. 1015, Dec. 1994.

[7] A. L. Swindlehurst and P. Stoica, "Maximum likelihood methods in radar array signal processing," *Proc. IEEE*, vol. 86, pp. 421–441, Feb. 1998.

[8] J. Ward, "Cramér-Rao bounds for target angle and Doppler estimation with space-time adaptive processing radar," in *Proc. 29th Asilomar Conf. Signals, Syst. Comput.*, Pacific Grove, CA, Nov. 1995, pp. 1198–1202.

[9] A. Dogandžić and A. Nehorai, "Cramér-Rao bounds for estimating range, velocity, and direction with a sensor array," in *Proc. 1st IEEE Sensor Array Multichannel Signal Process. Workshop*, Cambridge, MA, Mar. 2000, pp. 370–374.

[10] A. Dogandžić and A. Nehorai, "Estimating range, velocity, and direction with a radar array," in *Proc. Int. Conf. Acoust., Speech, Signal Process.*, Phoenix, AZ, Mar. 1999, pp. 2773–2776.

[11] S. Pasupathy and A. N. Venetsanopoulos, "Optimum active array processing structure and space-time factorability," *IEEE Trans. Aerosp. Electron. Syst.*, vol. AES-10, pp. 770–778, Nov. 1974.

[12] B. Hochwald and A. Nehorai, "Polarimetric modeling and parameter estimation with applications to remote sensing," *IEEE Trans. Signal Processing*, vol. 43, pp. 1923–1935, Aug. 1995.

[13] J. J. Blanz, A. Papathanassiou, M. Haardt, I. Furió, and P. W. Baier, "Smart antennas for combined DOA and joint channel estimation in time-slotted CDMA mobile radio systems with joint detection," *IEEE Trans. Veh. Technol.*, vol. 49, pp. 293–306, Mar. 2000.

[14] J. M. F. Moura, "Passive systems theory with narrow-band and linear constraints: Part III—Spatial/temporal diversity," *IEEE J. Oceanic Eng.*, vol. OE-4, pp. 113–119, July 1979.

[15] S. M. Kay, *Fundamentals of Statistical Signal Processing: Estimation Theory*. Englewood Cliffs, NJ: Prentice-Hall, 1993.

[16] M. J. D. Rendas and J. M. F. Moura, "Ambiguity in radar and sonar," *IEEE Trans. Signal Processing*, vol. 46, pp. 294–305, Feb. 1998.

[17] J. M. F. Moura and A. B. Baggeroer, "Passive systems theory with narrow-band and linear constraints: Part I—Spatial diversity," *IEEE J. Oceanic Eng.*, vol. OE-3, pp. 5–13, Jan. 1978.

[18] J. M. F. Moura, "Passive systems theory with narrow-band and linear constraints: Part II—Temporal diversity," *IEEE J. Oceanic Eng.*, vol. OE-4, pp. 19–30, Jan. 1979.
[19] A. W. Rihaczek, *Principles of High-Resolution Radar*. New York: McGraw-Hill, 1969.
[20] L. Cohen, *Time-Frequency Analysis*. Englewood Cliffs, NJ: Prentice-Hall, 1995.
[21] T. H. Glisson, C. I. Black, and A. P. Sage, "On sonar signal analysis," *IEEE Trans. Aerosp. Electron. Syst.*, vol. AES-6, pp. 37–50, Jan. 1970.
[22] B. R. Mahafza, *Introduction to Radar Analysis*. Boca Raton, FL: CRC, 1998.
[23] M. Hawkes and A. Nehorai, "Effects of sensor placement on acoustic vector-sensor array performance," *IEEE J. Oceanic Eng.*, vol. 24, pp. 33–40, Jan. 1999.
[24] R. O. Nielsen, "Azimuth and elevation angle estimation with a three-dimensional array," *IEEE J. Oceanic Eng.*, vol. 19, pp. 84–86, Jan. 1994.
[25] D. H. Johnson and D. E. Dudgeon, *Array Signal Procesing: Concepts and Techniques*. Englewood Cliffs, NJ: Prentice-Hall, 1993.
[26] L. D. Landau and E. M. Lifshitz, *Course of Theoretical Physics—Mechanics*, 2nd ed. Oxford, U.K.: Pergamon, 1969, pt. I.
[27] J. Frank and K. W. O'Haver, "Phased array antenna development at the Applied Physics Laboratory," *Johns Hopkins APL Tech. Dig.*, vol. 14, no. 4, pp. 339–347, 1993.
[28] X. Huang, J. P. Reilly, and M. Wong, "Optimal design of linear array of sensors," in *Proc. Int. Conf. Acoust., Speech, Signal Process.*, Toronto, ON, Canada, May 1991, pp. 1405–1408.
[29] A. A. Oliner and G. H. Knittel, *Proc. Phased Array Antenna Symp.*, Dedham, MA, 1972.
[30] A. K. Chan, A. Ishimaru, and R. A. Sigelmann, "Equally spaced spherical arrays," *Radio Sci.*, vol. 3, pp. 401–404, May 1968.
[31] E. Kiuchi and I. Ueda, "Tactical cylindrical active phased array radar," in *Proc. IEEE Int. Symp. Phased Array Syst. Technol.*, Tokyo, Japan, Oct. 1996, pp. 222–225.
[32] D. Loffler, E. Gschwendtner, and W. Wiesbeck, "Design and measurement of conformal antennas on cylindrical and spherical geometries," in *Proc. IEEE Africon*, Cape Town, South Africa, Oct. 1999, pp. 1005–1010.
[33] K. Kalliola, H. Laitinen, L. I. Vaskelainen, and P. Vainikainen, "Real-time 3-D spatial-temporal dual-polarized measurement of wideband radio channel at mobile station," *IEEE Trans. Instrum. Meas.*, vol. 49, pp. 439–448, Apr. 2000.
[34] C. Alakija and S. P. Stapleton, "A mobile base station phased array antenna," in *IEEE Int. Conf. Selected Topics Wireless Commun.*, Vancouver, BC, Canada, June 1992, pp. 118–121.
[35] A. Dogandžić and A. Nehorai, "Space-time fading channel estimation and symbol detection in unknown spatially correlated noise," , submitted for publication.
[36] H. Bunke and O. Bunke, "Identifiability and estimability," *Math. Operationsforsch. Statist.*, vol. 5, pp. 223–233, 1974.
[37] A. Wald, "Tests of statistical hypotheses concerning several parameters when the number of observations is large," *Trans. Amer. Math. Soc.*, vol. 54, pp. 426–482, 1943.
[38] C. R. Rao, *Linear Statistical Inference and Its Applications*, 2nd ed. New York: Wiley, 1973.
[39] E. F. Vonesh and V. M. Chinchilli, *Linear and Nonlinear Models for the Analysis of Repeated Measurements*. New York: Marcel Dekker, 1997.

Aleksandar Dogandžić (S'96) received the Dipl. Ing degree in electrical engineering from the University of Belgrade, Belgrade, Yugoslavia, in 1995 and the M.S. degree in electrical engineering and computer science from the University of Illinois, Chicago (UIC) in 1997, where he is pursuing the Ph.D. degree.

His research interests are in statistical signal processing and its applications to biomedicine, antenna arrays, and wireless communications.

Mr. Dogandžić received the Distinguished Electrical Engineering M.S. Student Award from the Chicago Chapter of the IEEE Communications Society. In 1997, he was awarded the Aileen S. Andrew Foundation Graduate Fellowship by the Department of Electrical Engineering and Computer Science at UIC. He is currently the recepient of the UIC University Fellowship.

Arye Nehorai (S'80–M'83–SM'90–F'94) received the B.Sc. and M.Sc. degrees in electrical engineering from the Technion—Israel Institute of Technology, Haifa, in 1976 and 1979, respectively, and the Ph.D. degree in electrical engineering from Stanford University, Stanford, CA, in 1983.

After graduation, he worked as a Research Engineer for Systems Control Technology, Inc., Palo Alto, CA. From 1985 to 1995, he was with the Department of Electrical Engineering, Yale University, New Haven, CT, where he became an Associate Professor in 1989. In 1995, he joined the Department of Electrical Engineering and Computer Science, University of Illinois at Chicago (UIC), as a Full Professor. He is currently Chair of the Department's Electrical and Computer Engineering Division and is managing the creation of a new Electrical and Computer Engineering Department at UIC. He holds a joint professorship with the Bioengineering Department at UIC. His research interests are in signal processing, communications, and biomedicine.

Dr. Nehorai is Editor-in-Chief of the IEEE TRANSACTIONS ON SIGNAL PROCESSING. He is also a Member of the Publications Board of the IEEE Signal Processing Society and the Editorial Board of *Signal Processing*. He has previously been an Associate Editor of the IEEE TRANSACTIONS ON ACOUSTICS, SPEECH AND SIGNAL PROCESSING, the IEEE SIGNAL PROCESSING LETTERS, the IEEE TRANSACTIONS ON ANTENNAS AND PROPAGATION, the IEEE JOURNAL OF OCEANIC ENGINEERING, and *Circuits, Systems, and Signal Processing*. He served as Chairman of the Connecticut IEEE Signal Processing Chapter from 1986 to 1995 and is currently the Chair and a Founding Member of the IEEE Signal Processing Society's Technical Committee on Sensor Array and Multichannel (SAM) Processing. He was the co-General Chair of the First IEEE SAM Signal Processing Workshop held in 2000. He was co-recipient, with P. Stoica, of the 1989 IEEE Signal Processing Society's Senior Award for Best Paper. He received the Faculty Research Award from UIC College of Engineering in 1999. He has been a Fellow of the Royal Statistical Society since 1996.